JCB Journal of Cell Biology

ARTICLE

TMEM175 does not function as a proton-selective ion channel to prevent lysosomal over-acidification

Erika Riederer[1], Vedrana Mikusevic[2], Tuoxian Tang[1], Lillian Martin[1], Joseph A. Mindell[2], and Dejian Ren[1]

The acidic pH of lysosomes required for function is established by the electrogenic V-ATPase proton pump. How lysosomes prevent hyper-acidification by the pump is not well established. Recently, the Parkinson's disease (PD)-associated protein TMEM175 was proposed as a H^+-selective channel to leak protons to counter over-acidification. We rigorously address key findings and predictions of this model and show that, in the lysosome, TMEM175 predominantly conducts K^+ and is not a H^+-selective channel. The native lysosomal H^+ leak is remarkably small, ∼0.02 fA, strongly arguing against major contributions from an ion channel. The predominant effect of TMEM175 deficiencies is lysosomal alkalinization in challenged cells, which is further evidence arguing against TMEM175 as a H^+-selective channel and can be explained by K^+ conductance through TMEM175. Also, lysosomes can be hyper-acidified by manipulations in the presence or absence of TMEM175. Our studies clarify a basic lysosomal biological problem and provide insights into the working mechanism of TMEM175 and its contribution to PD pathology.

Introduction

Lysosomes play important roles in many processes such as cellular clearance, material recycling, membrane repair, exocytosis, and Ca^{2+} signaling ([Andrews, 2000; Galione et al., 2011; Kaushik and Cuervo, 2018; Mindell, 2012; Xu and Ren, 2015] for reviews). They are also key metabolic sensors and their surfaces serve as hubs for signaling networks centered around protein kinases such as mTOR and AKT, and transcription factor TFEB (Goul et al., 2023; Saxton and Sabatini, 2017; Settembre and Ballabio, 2014). Disturbances in lysosomal function are implicated in numerous diseases such as lysosomal storage diseases, Alzheimer's disease, and Parkinson's disease (PD; Ballabio and Gieselmann, 2009; Burbulla et al., 2017; Chang et al., 2017; Lie and Nixon, 2018; Platt et al., 2012). Decrease in lysosome-mediated protein degradation is also a hallmark of aging (Lopez-Otin et al., 2013; Rubinsztein et al., 2011). A key feature of the lysosome is its acidic pH (∼4.7) necessary for various enzymes to accomplish their degradative functions as well as active transport of materials powered by the proton concentration ($[H^+]$) gradient (Kolter and Sandhoff, 2005; Mellman, 1989; Riederer et al., 2023; Xu and Ren, 2015). Alteration of the lysosomal pH impairs key functional facets of lysosome biology including degradation, movement, and fusion events, as well as nutrient sensing (Ballabio and Bonifacino, 2020; Korolchuk et al., 2011; Settembre et al., 2013; Xu and Ren, 2015).

The main driver generating the necessary lysosomal $[H^+]$ is the H^+-ATPase (V-ATPase), which pumps H^+ into the lysosome as it hydrolyzes ATP (Mindell, 2012; Ohkuma et al., 1982). The V-ATPase is electrogenic; as H^+ accumulates in the lumen, the accumulating positively charged protons establish an inside-positive voltage which, when high enough, would prevent acidification (Casey et al., 2010; Harikumar and Reeves, 1983; Ohkuma et al., 1983). As such, there needs to be a flux of counterions to dissipate the buildup of membrane potential for the pump to achieve sufficient acidification. Lysosomes likely use both anion (Cl^-) influx and cation (K^+ and Na^+) efflux as counterion pathways (Cuppoletti et al., 1987; Mindell, 2012; Steinberg et al., 2010; Van Dyke, 1993). In mutant lysosomes lacking either the Na^+-permeable TPC channels or K^+-permeable TMEM175 channel, the organelles are alkalinized when the cells are challenged with starvation under which there is likely high demand for counterion flux (Cang et al., 2015; Cang et al., 2013; Wie et al., 2021).

In addition to sufficient acidification, lysosomes also must have a mechanism protecting against excessive hyper-acidification because, at equilibrium, the V-ATPase could potentially drive the pH as low as ∼4 (see Discussion; Casey et al., 2010; Grabe et al., 2000), a pH that would significantly limit the function of the organelle. Traditionally, the prevention of excessive hyper-acidification was thought to be a built-in function

[1]Department of Biology, University of Pennsylvania, Philadelphia, PA, USA; [2]Membrane Transport Biophysics Section, National Institute of Neurological Disorders and Stroke, National Institutes of Health, Bethesda, MD, USA.

Correspondence to Dejian Ren: dren@sas.upenn.edu; Erika Riederer: erikari@sas.upenn.edu.

https://doi.org/10.1083/jcb.202501145

of the V-ATPase whose efficacy is controlled in part by luminal pH and the electrochemical gradient across the organelle membrane. As the proton electrochemical gradient increases upon acidification and/or buildup of membrane potential (Ψ), the efficacy of the pump decreases drastically by up to ∼90% (Johnson et al., 2016; Kosmidis et al., 2022; Van Dyke, 1993). The chloride-proton antiporter, ClC-7, is the major Cl^- ion conductance in the lysosome (Graves et al., 2008), and movement of the Cl^- ion into the lysosome can help dissipate the membrane potential. Regulation of this conductance could therefore aid in regulating lysosomal pH. Indeed, ClC-7 is tonically inhibited by signaling lipid $PI(3,5)P_2$; depleting this lipid leads to ClC-7 activation and lysosomal hyper-acidification, implicating this "counterion conductance" in lysosomal pH regulation (Leray et al., 2022).

A recent publication by Hu et al. proposed a new mechanism for the prevention of excessive hyper-acidification (Hu et al., 2022). Specifically, Hu et al. propose that lysosomes have a highly selective H^+ channel (relative proton to potassium permeability P_H/P_K = 48,000), formed by the TMEM175 protein, that conducts a large H^+ leak (0.1–1 pA currents at "resting") and prevents over-acidification.

TMEM175 is a PD-related protein and was previously identified as a K^+ channel found in lysosomes (Cang et al., 2015; Lee et al., 2017; Oh et al., 2020; Wie et al., 2021). There is large variation in TMEM175 function among the population. For example, the p.M393T variation is found in ∼18% of the population and in as many as ∼30% in certain ethnic groups (Wie et al., 2021). This variation leads to ∼50% reduction in channel function, increases neuronal susceptibility to stress-induced damage, and is associated with increased odds of developing PD. In PD patients, this variation is associated with accelerated decline in motor and cognitive function (Wie et al., 2021). In contrast, another variation (p.Q65P), present in ∼8% of the general population, is a gain-of-function variation and is associated with a lower risk of developing PD (Wie et al., 2021). The bidirectional ability to regulate channel function and PD susceptibility makes the protein an excellent target for the treatment of neurodegenerative diseases.

The new H^+ channel–based mechanism proposed by Hu et al. implies a dramatically different role in lysosomal physiology for this fundamentally important protein. If correct, the new model predicts hyper-acidification in cells with TMEM175 loss of function and therefore suggests therapies involving increasing lysosomal H^+ leak and raising lysosomal pH to correct the defect. Previous results, though, suggest that TMEM175 defects might lead to increased lysosomal pH, and such therapies would be contraindicated (Wie et al., 2021). Thus, it is essential to carefully evaluate these competing hypotheses to guide further work on basic mechanisms and therapies for PD.

In this study, we rigorously re-examined the key findings that led to the model of TMEM175 as a H^+-selective channel. We report here that electrophysiological measurements demonstrate that, in the presence of physiological K^+ concentrations, lysosomal TMEM175 proton selectivity is low, comparable with canonical cation channels. Similarly, live cell experiments reveal that baseline levels of proton leakage are minimal and do not change upon TMEM175 knockout (KO), inconsistent with proton channel activity. Finally, pH measurements in a range of cell types with TMEM175 KOs reveal either no pH change or alkalinization, opposite to the prediction if the protein is a proton channel. Thus, we conclude that the primary function of lysosomal TMEM175 is to conduct K^+ not protons.

Results

K^+ suppresses H^+ permeation through TMEM175

TMEM175 is localized on endolysosomal membranes (Cang et al., 2015; Chapel et al., 2013; Schroder et al., 2007) and was initially described as a lysosomal K^+ channel when recorded from lysosomes, based on both electrophysiological and structural experiments (Brunner et al., 2020; Cang et al., 2015; Lee et al., 2017; Oh et al., 2020; Wie et al., 2021). In support of its role as a K^+ channel, lysosomes from TMEM175 KO cells lack the voltage-independent K^+ conductance detected in WT, and their membrane potential (Ψ) is insensitive to changes in $[K^+]$ (Cang et al., 2015).

Like many other organelle proteins, TMEM175 can be mistargeted to the plasma membrane when overexpressed in a heterologous expression system, allowing plasma membrane currents to be recorded using whole cell patch-clamp techniques. Recent studies by Hu et al. and others recorded large plasma membrane H^+ currents from cells in which TMEM175 is overexpressed to the plasma membrane ($TMEM175_{PM}$; Hu et al., 2022; Zhang et al., 2023; Zheng et al., 2022). The key finding in this work was that inward H^+ currents (H^+ in the bath moving into cytoplasm in whole cell configuration, equivalent to H^+ in the lumen moving into cytosol in lysosomes) were recorded in acidic conditions (pH 4.5). However, the bath solutions for these experiments contained H^+ as the only permeable cation, in the complete absence of K^+ (Hu et al., 2022), quite unlike the conditions expected in the native lysosome lumen (Morgan et al., 2011). It is well-known that for many ion channels on the plasma membrane, removal of the preferred cation leads to anomalous conduction of alternate ions. For example, the highly Ca^{2+}-selective Ca_V channels become non-selective in the absence of extracellular divalent ions Ca^{2+} and Mg^{2+} (Almers and McCleskey, 1984; Hess and Tsien, 1984). Similarly, several plasma membrane K^+ channels have been shown to lose selectivity and to conduct Na^+ or become "defunct" with impaired conductivity in the absence of extracellular K^+ (Almers and Armstrong, 1980; Eisenman et al., 1986; Hoshi and Armstrong, 2013; Korn and Ikeda, 1995; Loboda et al., 2001; Ma et al., 2011; Pardo et al., 1992; Shin et al., 2005; Starkus et al., 1997; Wang et al., 2019; Ye et al., 2010).

It is, therefore, important to evaluate the contribution of the $TMEM175_{PM}$ proton conductance in the presence of K^+. Like Hu. et al. (2022), we observed H^+ currents in external solutions with H^+ as the only cation (replacing other cations with NMDG) when recording whole cell currents at the plasma membrane in transfected HEK293T cells. After forming a patch at pH 7.2, decreasing pH from 7.2 (0.06 μM H^+) to 4.5 (32 μM H^+) induced an inward current, consistent with previous observations (Fig. 1, A–C). These conditions leave the outward K^+ currents mostly

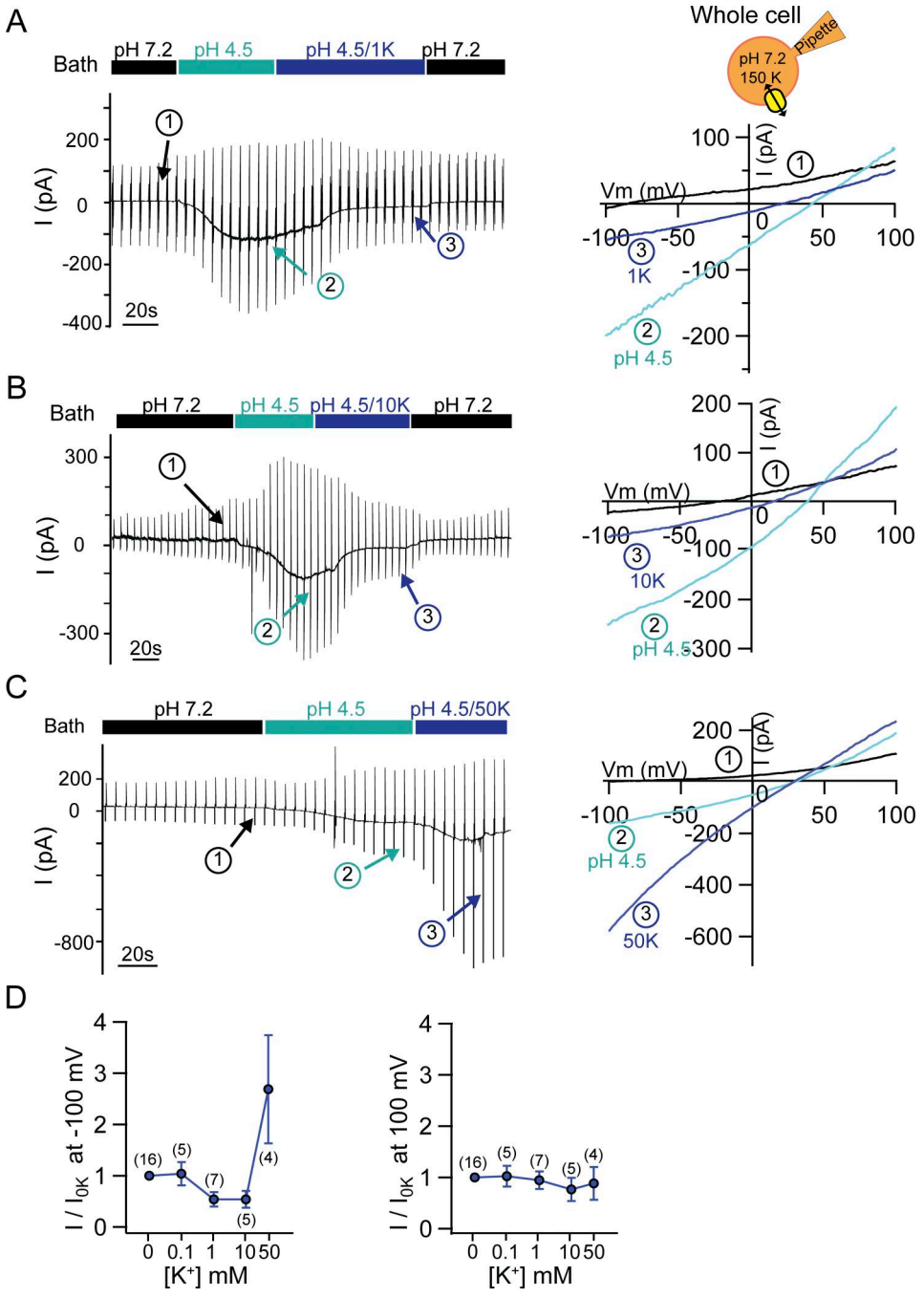

Figure 1. **K⁺ suppresses TMEM175-mediated H⁺ conductance.** Whole cell plasma membrane currents were recorded from TMEM175-transfected HEK293T cells using gap-free recording with a ramp from −120 to +120 mV (before LJP correction) at 400 ms, every 10 s (holding potential V_h = 0 mV) with pipette solution containing 150 mM K⁺, pH 7.2 ([H⁺] = 0.063 µM), and bath with varying [K⁺] and pH. Each cell was first recorded in a pH 7.2 bath containing no K⁺, followed a K⁺-free bath with pH 4.5 ([H⁺] = 31.62 µM), and baths containing varying amount of K⁺ as indicated. **(A–C)** Left: Representative traces of gap-free recording in bath with varying [K⁺] and pH as indicated. Right: Current–voltage (*I–V*) relationships obtained from ramps at time points indicated in the traces. **(D)** Amplitudes of inward (left, at −100 mV) and outward (right, at +100 mV) currents obtained using baths with varying [K⁺] normalized to that obtained with the immediately preceding pH 4.5 K⁺-free bath. For inward currents, the amplitudes of currents obtained with 1 mM K⁺-, 10 mM K⁺-, and 50 mM K⁺-containing baths normalized to that obtained with K⁺-free bath are 0.54, 0.54, and 2.69, respectively (all with the same [H⁺]/pH). Since the current amplitude of 50 mM K⁺-containing bath is 5.0× (=2.69/0.54) that with 10 mM K⁺-containing bath, one can estimate that, with 50 mM K⁺ in the bath, the fraction of K⁺ currents is 80% (= [5.0–1]/5.0). This estimate assumes that all the current obtained with 10 mM K⁺-containing bath is from H⁺ and the H⁺ current remained the same size in 50 mM K⁺-containing bath, which likely overestimates the contribution by H⁺ and underestimates the fraction of K⁺ currents. LJP was adjusted offline. Error bars are SEM and the number in parenthesis is the number of recordings in each condition. Mock (empty-vector)-transfected HEK293T cells had minimal inward currents under similar recording conditions with pH 4.5 bath containing 0 mM K⁺ (−9.8 ± 2.5 pA at −100 mV, n = 6), 1 mM K⁺ (−19.1 ± 4.8 pA, n = 5), or 50 mM K⁺ (−39.5 ± 10.8 pA, n = 4).

unchanged (Fig. 1, A–C). The reversal potential (V_{rev}) of the current was 34.0 ± 2.9 mV, corresponding to a P_H/P_K of 18,845, again similar to that reported by Hu et al. (2022) at the plasma membrane (Hu et al., 2022; Zheng et al., 2022). However, adding just 1 mM K^+ in the bath suppressed the H^+ current by at least 46% and shifted V_{rev} to 13.9 ± 6.1 mV, corresponding to a reduction of P_H/P_K to 8,340 (Fig. 1, A and D). The degree of H^+ current suppression by K^+ is likely underestimated as the calculation assumes that all the inward current was carried by H^+ alone even with both H^+ (32 μM) and K^+ (1 mM) in the bath. Further raising [K^+] from 1 to 50 mM, likely closer to the physiological concentration of K^+ in the lysosome lumen (Ohkuma et al., 1983; Steinberg et al., 2010), increased the total inward current by ∼500%, suggesting that the H^+ conductance contributes even less because most of the permeant ion is K^+ (>80%, Fig. 1 D, assuming the H^+ current remained the same when bath [K^+] was increased from 1 to 50 mM), in strong contrast to the proposal by Hu et al. that H^+ constitutes >90% of the permeant ions through TMEM175 (Hu et al., 2022). Another indicator of the complex interactions between K^+ and H^+ currents is the relationship between current (I) and [K^+], an inverted bell-shaped curve consistent with an anomalous mole fraction effect similar to those observed in Ca_V and K^+ channels (Fig. 1 D; Eisenman et al., 1986; Hess and Tsien, 1984; Korn and Ikeda, 1995). Thus, the apparently large plasma membrane H^+ conductance and high P_H/P_K in experiments with H^+ as the only current carrier are, at least in part, due to the lack of inhibition and competition by physiological [K^+].

Proton selectivity of lysosomal TMEM175

Hu et al. concluded that TMEM175 is highly proton selective with a P_H/P_K of 48,000 (Hu et al., 2022), in the range of selectivities of the well-established H^+ channels such as H_V1 ($P_H/P_{Na} > 10^6$) and Otop1 ($P_H/P_{Na} > 10^5$; Decoursey, 2003; Tu et al., 2018). Intriguingly, Hu et al. presented P_H/P_K data measured only from TMEM175 mistargeted to the plasma membrane but not from recordings conducted using lysosomes. Since the lipid and geometric conditions are quite different in the plasma membrane than in the lysosome, it is important to determine the selectivity in the lysosomal membrane itself.

The initial characterization of TMEM175 using whole-organelle patch-clamp recordings to record currents through TMEM175 in the lysosomal membrane suggested that TMEM175 is a K^+-conducting channel. Reversal potential measurements in lysosomes from multiple cell types (macrophage, neurons, glia, cardiac myocytes, fibroblasts, and HEK293T cells) revealed values close to the equilibrium potential for K^+ and far from that of H^+, suggesting that the channel primarily conducts K^+, not H^+ (Cang et al., 2015; Cang et al., 2014; Wie et al., 2021). In addition, varying bath [K^+] during recording from TMEM175-transfected lysosomes led to large changes in the reversal potential (Cang et al., 2015; Wie et al., 2021), in stark contrast to the minimal effect of such manipulations on H^+-selective channels such as Otop1 (Tu et al., 2018). These findings were rejected by Hu et al. as having been conducted at "nonphysiological" "neutral" pH even though the actual pH was 4.6 or 5.5, close to the native lysosomal pH (∼4.5–5.5 at resting and higher during acidification).

Nevertheless, we sought to reproduce and extend these measurements. To further probe the H^+ selectivity of lysosomal TMEM175, we recorded whole organelle currents from lysosomes of TMEM175-transfected cells using pipette solutions at pH 4.6 (Fig. 2). The current sizes were generally smaller than those recorded with a pH 5.5 pipette (Cang et al., 2015; Wie et al., 2021), consistent with previous finding that low pH inhibits TMEM175 mistargeted onto the plasma membrane (Zheng et al., 2022). In conditions analogous to the whole cell recording condition used by Hu et al. (2022) to determine P_H/P_K, with only H^+ as the permeant cation in both pipette (lumen, pH 4.6) and bath (cytosol equivalent, pH 7.2), we observed a small, but detectable, inward H^+ current at large negative potentials from lysosomes (−9.4 ± 4.9 pA at −100 mV, n = 5, Fig. 2 B, black trace). This current is TMEM175 specific as it was largely absent in non-transfected lysosomes (−1 ± 0.72 pA at −100 mV, Fig. S1). Adding a physiological concentration of K^+ (150 mM) to the cytosol-equivalent bath induced outward K^+ currents, suggesting TMEM175 conduction of K^+. Furthermore, the addition of K^+ also reduced the inward current by 70%, −2.8 ± 1.4 pA (Fig. 2 B). The presumed inhibition of H^+ exit from the lysosomal lumen by cytosolic K^+ indicates that K^+ ions permeating the TMEM175 pore from outside the lysosome are sufficient to largely block access to protons from the lumen. Since the cytosolic K^+ concentration rarely drops below ∼150 mM, proton exit is unlikely to be a major factor in physiological conditions.

With 150 mM K^+ in the bath, lysosomal TMEM175 currents reversed polarity at −93.5 ± 13.9 mV (n = 5). This reversal potential (Ψ_{rev}) is drastically (by 144.7 mV) different from the Ψ_{rev} of +51.2 mV predicted for a highly H^+-selective TMEM175 (P_H/P_K of 48,000, Fig. 2, B and E). Using the Goldman–Hodgkin–Katz (GHK) equation, we estimate the P_H/P_K of lysosomal TMEM175 at 137. This low P_H/P_K is comparable with the values for canonical ion channels that are largely permeable to other ions, such as the voltage gated Na^+ channel (P_H/P_{Na} of ∼250 [Mozhayeva and Naumov, 1983]). These values, however, are several orders of magnitude lower than those of H^+-selective channels such as Otop1 and H_V1 (Decoursey, 2003; Tu et al., 2018). Thus, lysosomal TMEM175 is not a H^+-selective channel. Previous conclusions of high H^+ selectivity of TMEM175 may result from mistargeting the protein to the plasma membrane, which has different lipid composition and membrane curvature than those of lysosomal membranes.

We next examined the effects of luminal K^+ on TMEM175 conductance. With a sub-physiological 5 mM K^+ in the pipette (lumen), the amplitudes of inward (lumen to cytosol) currents at −100 mV were increased from −9.4 ± 4.9 to −26.9 ± 15.7 pA (Fig. 2 C). When luminal [K^+] was increased to 50 mM, close to the physiological K^+ levels (Ohkuma et al., 1983; Steinberg et al., 2010), the inward currents were increased to −31.6 ± 6.6 pA (Fig. 2, B and D), likely due to an increase in K^+ conduction. Ψ_{rev} obtained with 50 mM luminal K^+ and 150 mM K^+ in the bath was −24.9 ± 4.8 mV, corresponding to a P_H/P_K of 197 (Fig. 2 E). Given that the TMEM175 K^+ conductance is voltage-independent (measured in both plasma and lysosomal membranes; Cang

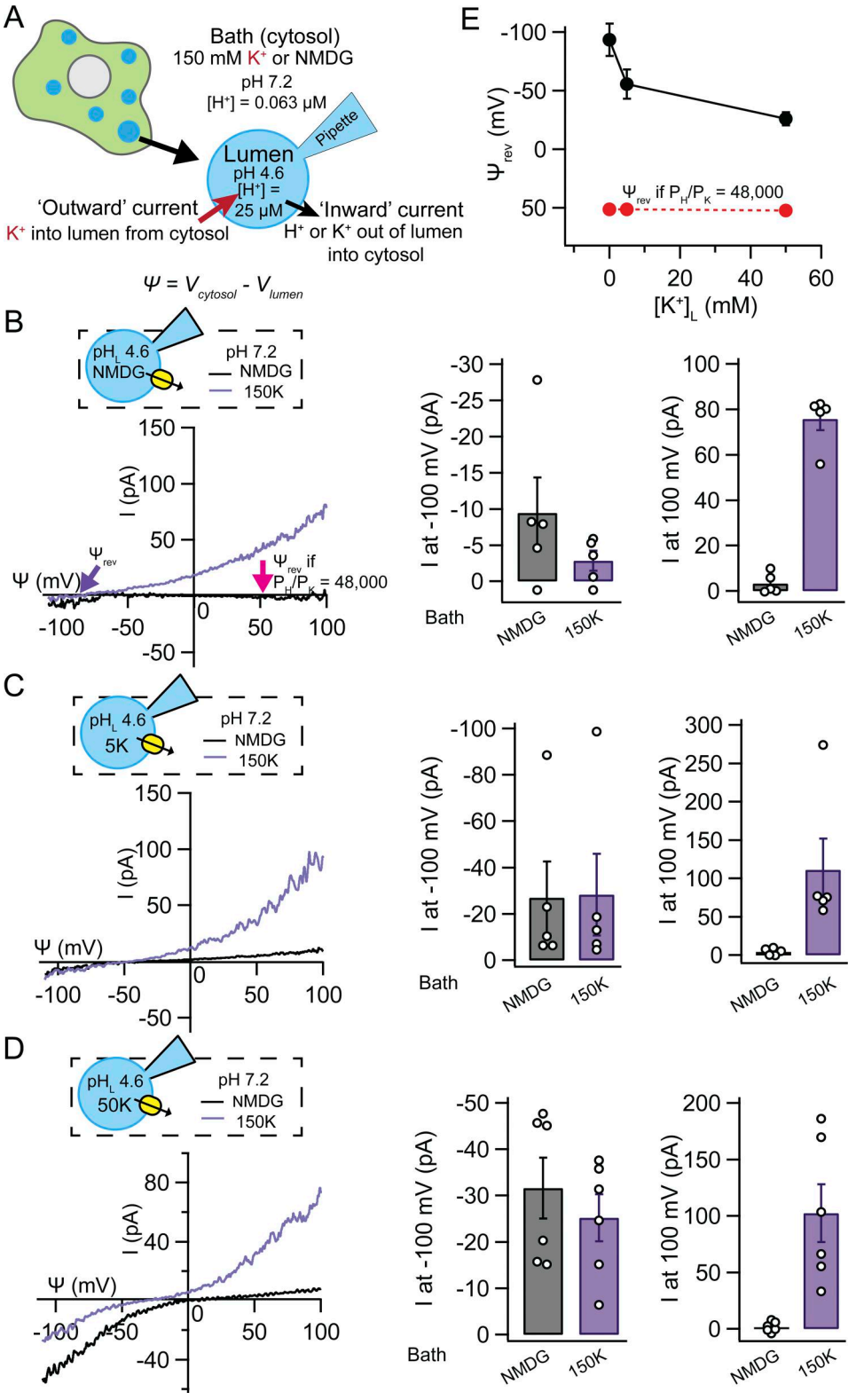

Figure 2. **Lysosomal TMEM175 is not a H⁺-selective channel. (A)** Schematic for whole organelle recording from lysosomes dissected from TMEM175-transfected HEK293T cells. The definitions of membrane potential (ΔΨ or Ψ) and current (*I*) followed a previously proposed nomenclature (Bertl et al., 1992). Ψ (= $V_{cytosol}$ − V_{lumen}) is the voltage across the lysosomal membrane with lumen used as a reference. "Inward" cation current denotes cations leaving the lumen into the cytosol (bath), while "outward" cation current denotes entering the lumen from the cytosol (bath). *I*-Ψ relationships were obtained with a ramp protocol from −120 to +120 mV in 1 s, Ψ_h = 0 mV (before LJP adjustment). Pipette and bath solutions had pH 4.6 and pH 7.2, respectively. **(B–D)** Currents recorded with bath solutions containing 0 mM K⁺ (NMDG-containing) or 150 mM K⁺ and pipette solutions containing 0 mM (B), 5 mM (C), or 50 mM (D) K⁺. For each pipette condition, representative traces recorded with NMDG-containing and 150 mM K⁺-containing baths from the same lysosome are shown on the left. Summaries

of the inward (at −100 mV) and outward (at +100 mV) current amplitudes are on the middle and right, respectively. Each circle represents data from one lysosome. The number of lysosomes in each pipette condition are n = 5 for B and C and n = 6 for D. The pink arrow in B indicates the Ψ_{rev} for 150 mM K^+-containing bath if the P_H/P_K were 48,000, as previously reported by Hu et al., while the purple arrow indicates the measured Ψ_{rev}. LJP was adjusted offline. **(E)** Average reversal potentials obtained with 150 mM K^+-containing bath and pipette (lumen) solutions containing 0, 5, or 50 mM K^+. The number of lysosomes for determination of Ψ_{rev} for each pipette conditions containing 0 and 5 mM K^+ are n = 5 and n = 6 for pipette containing 50 mM K^+. The red dots and dashed red line indicate predicted reversal potentials under each condition if the channel were a H^+-selective channel with P_H/P_K of 48,000, as proposed by Hu et al. (2022). Error bars are SEM.

et al., 2015; Lee et al., 2017; Wie et al., 2021; Zheng et al., 2022), the much larger outward K^+ currents at +100 mV than the inward currents at −100 mV also suggest that H^+ currents likely constitute only a very small fraction of the inward currents through TMEM175.

Lysosomal pH does not readily reach below pH 4.0 because of the inhibition of the V-ATPase at low pH (Johnson et al., 2016; Kosmidis et al., 2022; Van Dyke, 1993). To probe whether TMEM175's role might increase at this low pH, we measured lysosomal TMEM175 currents with pH 4.0 pipette solution to maximize the contributions of proton conduction. These currents were similar to those recorded with pH 4.6 in the pipette (Fig. S2). The inward H^+ currents with K^+-free bath and pipette were slightly larger than those recorded with a pipette pH of 4.6. The currents with 150 mM K^+ in the bath reversed at −71 mV (Fig. S2, A and C), corresponding to P_H/P_K of ∼85, again inconsistent with TMEM175 being a H^+-selective channel. The increase of inward H^+ currents when pipette pH was decreased from 4.6 to 4 is expected from an approximately fourfold increase in luminal [H^+] but provides no evidence that the channel is activated/gated by low pH, similar to the conclusion by Zheng et al., who recorded H^+ currents from TMEM175 mistargeted onto the plasma membrane and concluded that "TMEM175 is constitutively active and is not gated by pH" (Zheng et al., 2022). In fact, low pH inhibits TMEM175 (Zheng et al., 2022).

Proton permeability and selectivity of lysosomal TRPML1

Proton permeability is commonly found in lipid membranes and ion channels such as Na_V channels (Mozhayeva and Naumov, 1983), TRPV1 (Caterina et al., 1997; Hellwig et al., 2004), and TRPM7 (Jiang et al., 2005; Numata and Okada, 2008), partly because of the smaller diameter of H^+ than those of other ions (Decoursey, 2003). The TRPML1 channel ubiquitously expressed in mammalian lysosomes was previously reported to also conduct H^+ when tested at the plasma membrane (Soyombo et al., 2006), though the channel has also been suggested to be proton impermeable in lysosomes (Hu et al., 2022). We sought to determine whether TRPML1 might contribute to any proton currents by recording from TRPML1-transfected lysosomes. Even without activating the channel with $PI(3,5)P_2$, an endolysosome-localized lipid required for the optimal function of TRPML1 (Dong et al., 2010), the H^+ current was prominent (−41.4 ± 13.9 pA, at −100 mV, n = 5), much larger than that from TMEM175-transfected lysosomes under identical recording conditions (Fig. 2 B). The addition of 1 µM $PI(3,5)P_2$ in the bath drastically increased the currents to −149.5 ± 29.4 pA (n = 5, Fig. 3 A). Under a "bi-ionic" condition with 150 mM K^+ in the bath (Fig. 3 B), the Ψ_{rev} was −84.3 ± 7.1 mV, corresponding to a P_H/P_K of 199, comparable with that of TMEM175 but much lower than those of H^+-selective channels. Thus, lysosomal TRPML1 is also able to conduct H^+ although it is not a H^+-selective channel.

Lysosomal H^+ leak in live cells

We extended our findings from patch-clamp recording by examining the channel's relative contribution to H^+ leak in native lysosomes in intact cells using live cell imaging, a less intrusive approach than patch-clamp of isolated lysosomes. We estimated the contribution of H^+ leaks by examining the rate of lysosomal pH increase after inhibiting the V-ATPase H^+ pump and subsequent addition of a weak base (Fig. 4, A and B; Johnson et al., 2016). To monitor the pH changes in situ, we used the ratiometric dye, dextran-conjugated Oregon Green 488 (OG), which has a pKa of ∼4.8, well suited for the range of lysosomal pH (DiCiccio and Steinberg, 2011; Steinberg et al., 2010). The measured H^+ leak (in concentration) is the product of the rate of pH change and the buffering capacity, which is determined with the addition of ammonium chloride. The lysosomes H^+-leak currents were estimated to be ∼0.017 fA (∼104 protons/s, assuming a 300 nm lysosome diameter; Fig. 4 E). This remarkably small conductance (∼0.1 fS, assuming driving force of ∼200 mV for H^+, see Discussion) is comparable with minimal nonspecific proton leaks through lipid bilayer membranes but unlikely from high conduction rates of ion channels, which generally conduct 10^6 ions/s.

We evaluated the contribution of TMEM175 to the lysosomal H^+ leaks by performing similar measurements in lysosomes from TMEM175 KO mouse neurons and macrophages. In those experiments, the H^+-leak sizes are comparable with those in the WT (Fig. 4, C–E). Together, our live cell measurements thus reveal a remarkably small lysosomal H^+ leak which is unchanged in the absence of TMEM175.

Loss of TMEM175 in hippocampal neurons leads to lysosomal alkalinization, contrary to what is predicted by TMEM175 being a H^+-selective H^+-leak channel

If TMEM175 is a major H^+-leak pathway that limits lysosomal acidification, then knocking it out would be expected to induce lysosomal hyper-acidification. In contrast, if TMEM175 is primarily a K^+ channel, then knocking it out might lead to no change or alkalinization of lysosomal pH, based on the hypothesis that it has a role in conducting K^+ as a counterion (to dissipate the potential generated by V-ATPase activity). In our previous experiments with lysosomes in hippocampal neurons cultured from mice, we found that lysosomes in TMEM175 KO cells had a pH similar to that in WT when the cells were nutrient replete (Wie et al., 2021). However, KO lysosomes were alkalinized by ∼0.5 units (∼70% decrease in [H^+]) when the neurons were starved, a condition under which there is likely a higher

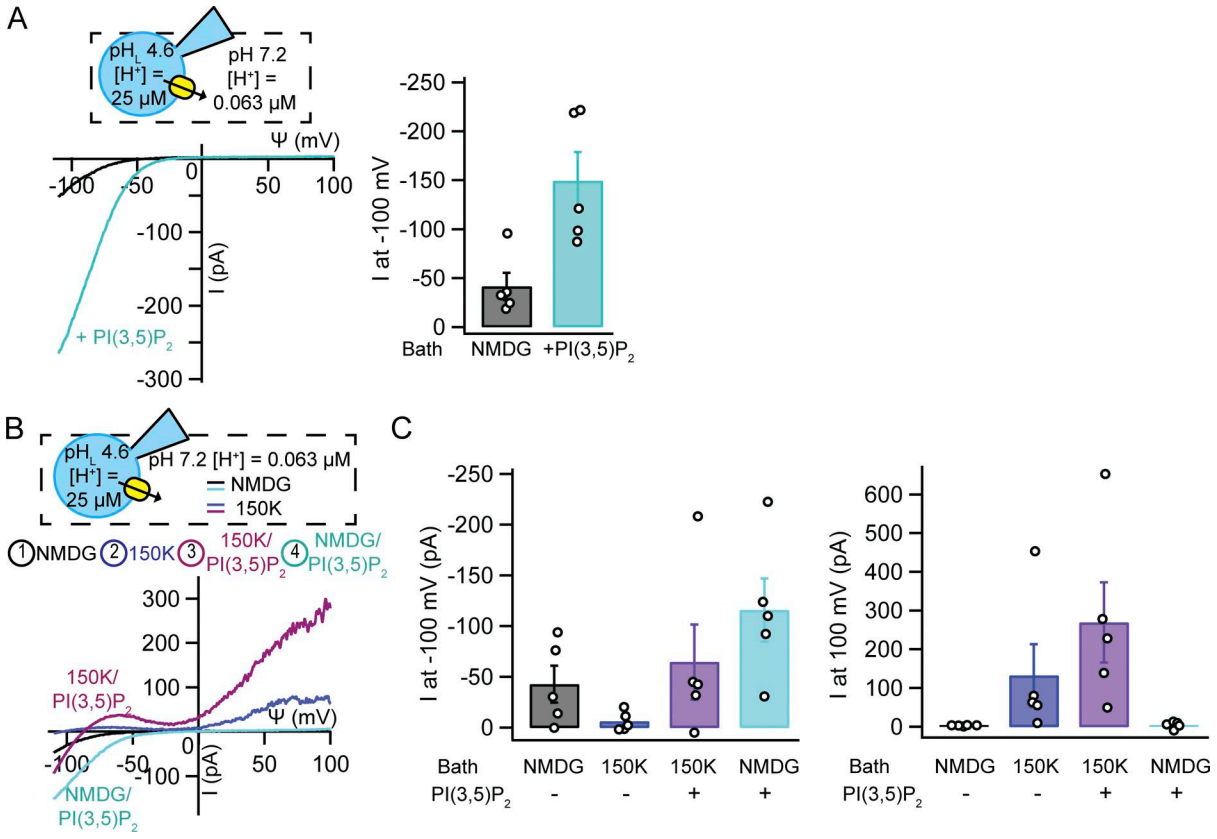

Figure 3. **Lysosomal TRPML1 is H⁺-permeable but not H⁺-selective.** Whole lysosome recordings from TRPML1-transfected HEK293T cells. Pipette solution contained NMDG but no K^+ (pH 4.6), and bath solutions (pH 7.2) contained no K^+ (NMDG-containing) or 150 mM K^+ as indicated. A voltage ramp protocol (−120 to +120 mV in 1 s, Ψ_h = 0 mV, before LJP correction) was used. **(A)** H^+ currents were recorded from each lysosome with a bath containing 150 mM NMDG followed by the addition of $PI(3,5)P_2$ (1 µM). Left: Representative traces. Right: Summary of current amplitudes at −100 and +100 mV. Each circle represents the current from a lysosome patch: n = 5. **(B and C)** Each lysosome was recorded with baths containing 150 mM NMDG or 150 mM K^+ with and without $PI(3,5)P_2$ (1 µM), in the sequence as indicated by circled numbers in B. **(B)** Representative I-Ψ relationships extracted from ramps under each condition. **(C)** Summary of inward (at −100 mV) and outward (at +100 mV) currents recorded in the four bath solutions outlined in B. Each circle represents one lysosome: n = 5. Error bars are SEM.

demand for lysosomal biological activity and, therefore, a higher demand for H^+ pumping and in K^+-mediated counterion flux. This alkalinization in the KO is opposite the expected effect if TMEM175 is a proton channel.

In contrast to these results, Hu et al. reported that lysosomes in hippocampal neurons cultured from their TMEM175 KO were hyper-acidified when the neurons were nutrient replete. It is unclear how to reconcile the difference between the findings. One possible reason is genetic background difference and potential off-targets resulting from CRISPR-mediated mutagenesis. The mice we used in our previous experiments were backcrossed for five generations and littermates were used as controls (Wie et al., 2021); backcrossing and control information was not provided by Hu et al. (2022).

To minimize genetic background complications, we have now carried out additional lysosomal pH analysis in two independent KO mouse lines that have been extensively backcrossed to C57BL6/J (Jax) for 10 or more generations in ∼8 years. These 2 lines (K1 and K3, Fig. 5 A) were derived from two different F0 founders and have different lengths of deletions (all out-of-frame). Littermates generated from mating between heterozygotes were used as control to further minimize complication by unwanted genetic background differences. In both the alleles, we found no hyper-acidification in hippocampal neuron lysosomes in the KO compared with WT (Fig. 5 C and Fig. S4 A). In fact, the KO lysosomes were drastically alkalinized (by ∼0.5 U) in both the lines upon starvation, as demonstrated by the dye signal ratios before calibration (Fig. 5 B) and average pH values (Fig. 5 D and Fig. S4 A). Alkalinization in the KO neurons was also consistent with lower fluorescence signals from LysoTracker, a non-ratiometric pH-sensitive dye that is less quantitative but requires no calibration (Fig. S3 B).

TMEM175 deficiency in mouse macrophages and human cells also leads to lysosomal alkalinization

As TMEM175 is ubiquitously expressed, we tested in other cells whether TMEM175 deficiency leads to lysosomal hyper-acidification, as predicted by a H^+-selective TMEM175 channel model. In peritoneal macrophages isolated from adult mice, we found no significant hyper-acidification in the KO when cells were nutrient replete, compared with those from the WT littermate control. Again, KO lysosomes

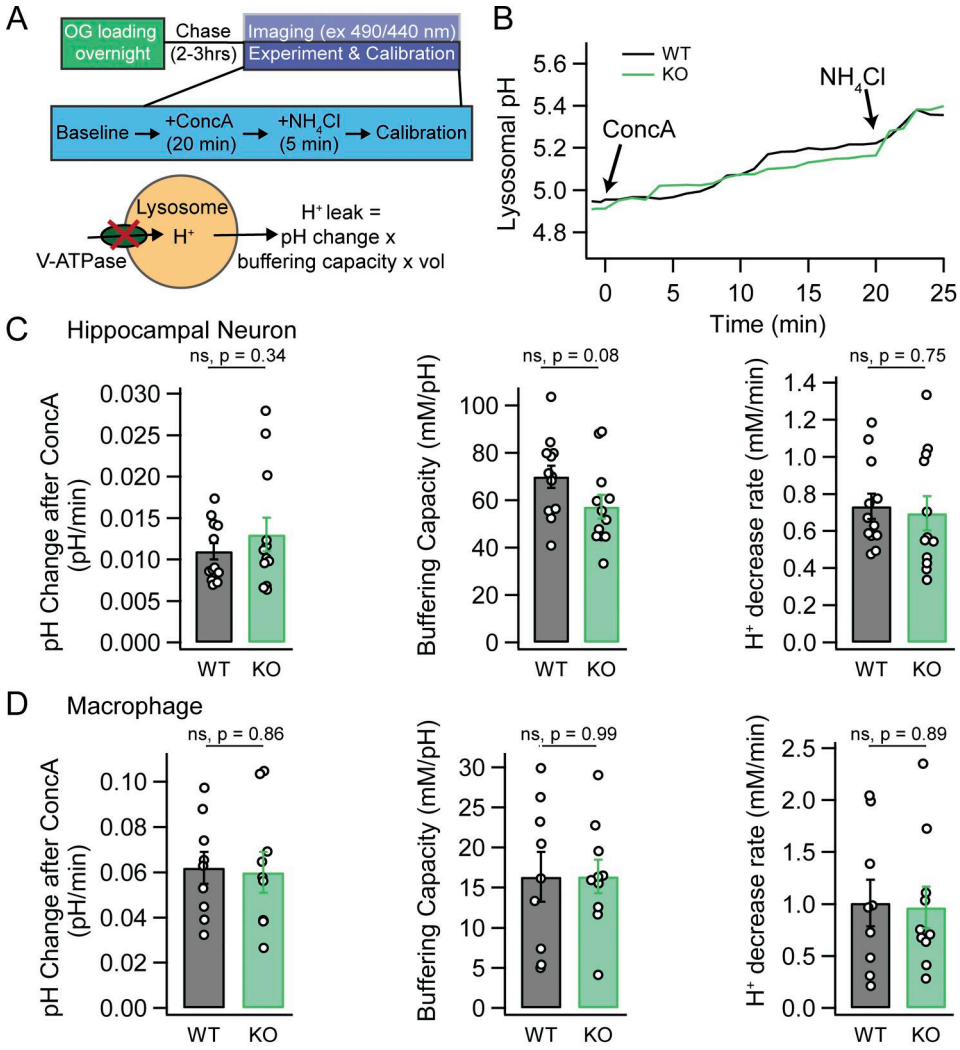

E

	Hippocampal Neurons		Macrophages	
	WT	KO	WT	KO
pH change (pH/min)	0.011 ± 0.001	0.015 ± 0.002	0.062 ± 0.007	0.060 ± 0.008
Buffering capacity (mM/pH)	70.1 ± 5	57.3 ± 5	16.3 ± 3	16.4 ± 2
[H+] decrease rate (mM/min)	0.732 ± 0.07	0.696 ± 0.09	1.01 ± 0.2	0.968 ± 0.2
H+ leak (moles/sec)*	1.72×10^{-22}	1.64×10^{-22}	2.38×10^{-22}	2.28×10^{-22}
H+ leak (protons/s)*	104	99	143	137
H+ leak (current, I_H (fA))*	0.017	0.016	0.023	0.022

Figure 4. **Lysosomal H+ leak is extremely small and is unlikely mediated by ion channels including TMEM175. (A)** Experimental procedure for measuring lysosomal H+ leak. Cells are loaded with OG followed by chase with fresh culture medium for 3 h (hippocampal neurons) or 2 h (peritoneal macrophages). The lysosomal pH is imaged before and continuously after V-ATPase blocker, concanamycin A (ConcA), is added to the cells (5 µM for neurons and 2 µM for macrophages) as well as after a weak base, NH_4Cl, is added to measure buffering capacity, followed by an in situ calibration for each coverslip. **(B)** Representative lysosomal pH changes of a cultured WT and TMEM175 KO hippocampal neuron in response to ConcA and NH_4Cl. **(C and D)** Summaries of the various parameters extracted from the experiment in hippocampal neurons (C) and macrophages (D) for WT and TMEM175 KO mice. There is no statistical significance between WT and KO cells in pH change over time, buffering capacity, or [H+] decrease rate with an unpaired two-tailed *t* test. Each circle represents one cell with *n* = 12 for WT and KO hippocampal neurons and *n* = 9 for WT and *n* = 10 for KO macrophages. Hippocampal neurons (C) are from three TMEM175 KO lines (K1, K3, and K6, as indicated in Fig. 5 legend), while macrophages (D) are from two TMEM175 KO lines (K1 and K3). H+ decrease rate (in mM/min) was calculated as the product between pH change rate (pH/min) and buffering capacity (mM/pH) for each cell. **(E)** Table of values from key parameters summarized in the previous bar graphs (C and D). * For total H+ leak of a lysosome, an assumption was made that lysosomes are spheres of 300-nm diameter and the calculated H+-leak values are based on the average [H+] decrease presented in the table. Error bars are SEM.

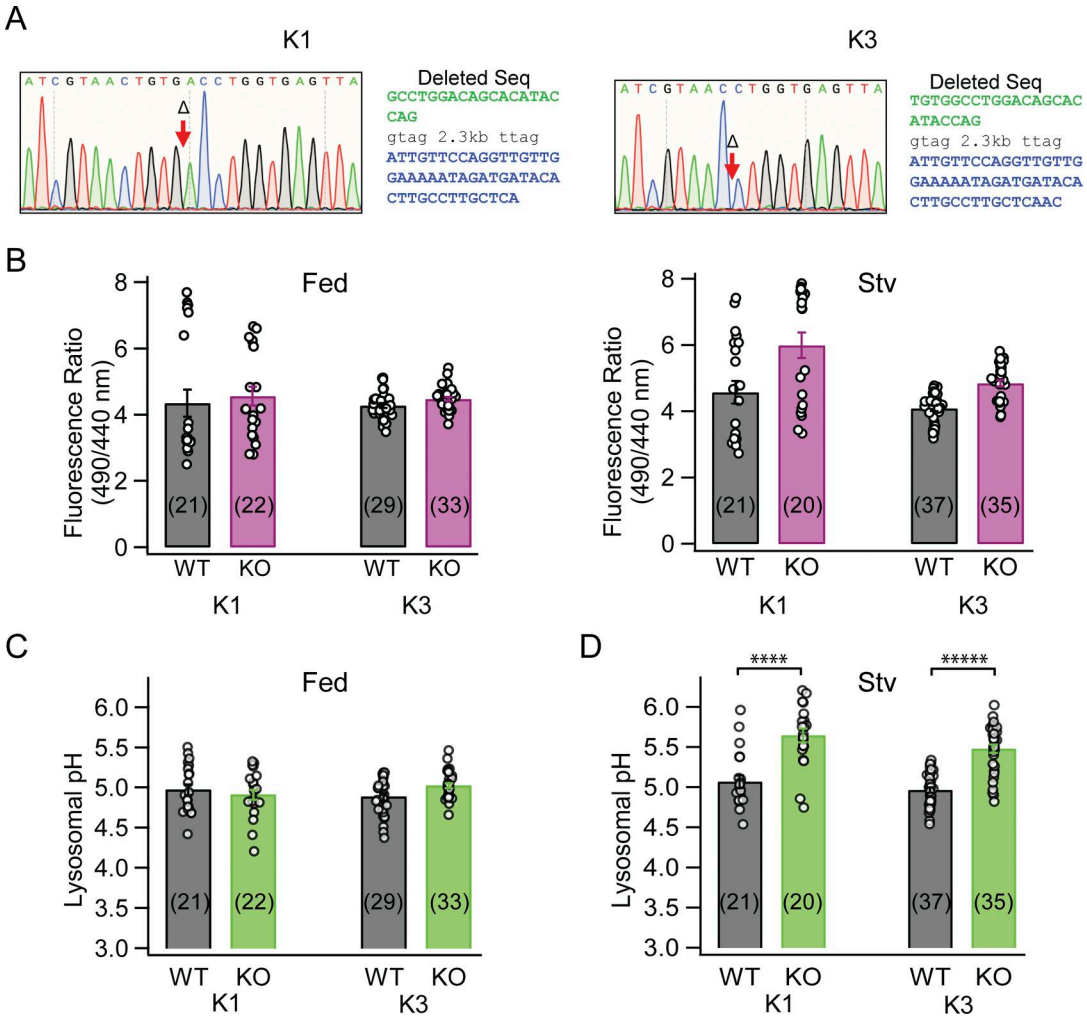

Figure 5. **Lack of TMEM175 results in lysosomal alkalinization, not hyper-acidification, in mouse hippocampal neurons. (A)** Sequence deletions in two independent TMEM175 KO mouse lines (K1, K3) used to determine lysosomal pH. Left: Sanger sequencing chromatograms with the deletion site in each allele indicated by an arrow. Right: sequences deleted in exons 3 (green), exon 4 (blue), and the intron between (lower case). Numbers of base pairs deleted in exons 3 and 4 in each allele are K1 (20 bp in exon 3 and 47 bp in exon 4) and K3 (24 bp in exon 3 and 49 bp in exon 4). Another line (K6, used in Fig. 4 and Fig. S3 B) has 23 bp deletion in exon 3 and 51 bp in exon 4. Partial sequences of WT in the region are 5′-TTCTAATCGTAACTGTGGCCTGGACAGCACATACCAGGTAG-3′ 2.3 kb 5′-TTAGATTGTTCCAGGTTGTTGGAAAAATAGATGATACACTTGCCTTGCTCAACCTGG-3′ (exon sequences are in capital; sequences targeted by the two guide RNAs used for the generation of KO mice are underlined). **(B)** Average ratios of fluorescence signal, before calibration, from excitation at 490 nm to that at 440 nm in OG-loaded hippocampal neurons cultured from WT and KO mice, with and without starvation. The starvation condition for neurons is overnight incubation without B-27 supplement. The number in parentheses is the number of cells with each circle representing the ratio for one cell and the corresponding mouse line (K1 or K3) is labeled. **(C and D)** Summary of the lysosomal pH of WT and KO hippocampal neurons cultured from two KO lines with (D) and without (C) starvation. The numbers in parentheses are the number of cells for each condition. Each circle represents the average of one neuron. See Fig. S4 A for lysosomal pH averaged from each individual animal. P values are from unpaired two-tailed *t* test, where **** is $P < 10^{-6}$ and ***** is $P < 10^{-7}$. Error bars are SEM.

are significantly alkalinized compared with the WT upon starvation challenge (Fig. 6 A, Fig. S3 A, and Fig. S4 C).

We further tested the role of TMEM175 in lysosomal pH in the HEK293T human cells by comparing WT and KO cell lines (Fig. S5). In two independent KO lines we developed (Fig. S5), there was no hyper-acidification compared with the parental WT line from which the KO lines were derived when the cells were nutrient replete. Again, under starvation challenge, presumably with a higher H^+-pumping activity which leads to a hyperpolarized membrane potential (lumen more positive) at which both Na^+ and K^+ can exit the lysosome as counterions (Riederer et al., 2023), the KO lysosomes, compared with WT, were alkalinized by ∼0.5 U (0.5 in one and 0.43 in the other; Fig. 6 B).

Lysosomes can be hyper-acidified in the presence or absence of TMEM175

Another prediction of the presence of a major H^+-selective leak channel, TMEM175, would be that lysosomes with TMEM175, which is ubiquitously expressed, cannot be hyper-acidified, as the leak from a channel would overpower the H^+-pumping capability of the V-ATPase, which is present in the quantity of only ∼1–2 functional molecules in each lysosome and pump only a few hundred H^+ ions per second (Maxson et al., 2022). However,

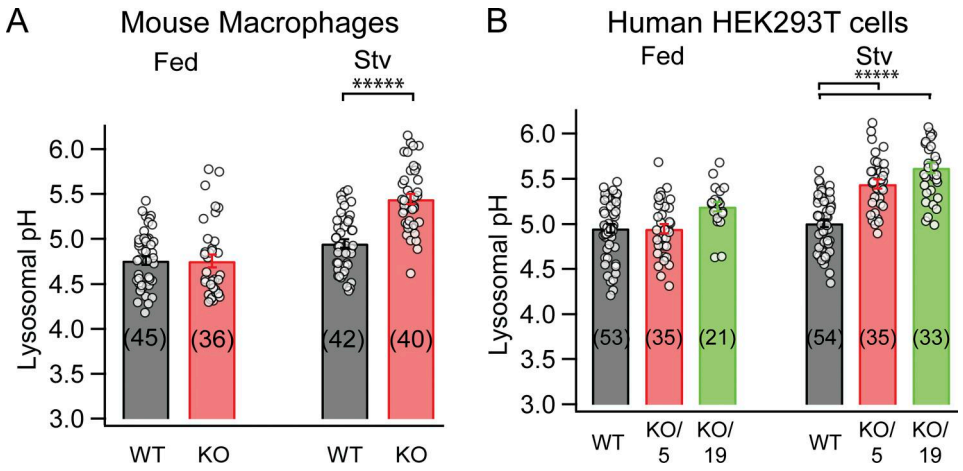

Figure 6. **TMEM175-deficient lysosomes from mouse macrophages and human cells are hypo-acidified. (A and B)** The lysosomal pH of cultured extracted peritoneal mouse macrophages (A) from WT and TMEM175 KO mice, as well as cultured WT and TMEM175 KO HEK293T human cells (B). Macrophages were cultured from adult mice from the K1 and K3 TMEM175 KO lines. For HEK293T cells (B), two independent KO lines (KO/5 and KO/19) with different deletions were tested (see Fig. S5 for sequences deleted in each line). The numbers in parenthesis are the number of cells in each condition. P values are from unpaired two-tailed *t* test, where * is $P < 0.05$ and ***** is $P < 10^{-7}$. Error bars are SEM.

hyper-acidification of resting lysosomes has been found in several mutant mouse lines and human cells that presumably have increased Cl^- influx (CLC-7 gain-of-function mutants [Leray et al., 2022; Nicoli et al., 2019]), or increased Na^+ efflux (TPC2 gain-of-function mutant [Wang et al., 2023]), an observation inconsistent with the presence of a large proton leak.

The idea that TMEM175 functions as a H^+-leak channel predicts not only that WT lysosomes cannot be hyper-acidified but also that TMEM175 KO lysosomes would be more easily hyper-acidified since the proton leak would be absent. We tested the two predictions in the human embryonic kidney cell line HEK293T and the human osteosarcoma cell line U2OS using apilimod, a PIKfyve inhibitor shown to cause lysosomal hyper-acidification by relieving $PI(3,5)P_2$-mediated inhibition of CLC-7 (Leray et al., 2022). As in HEK293T cells, knocking out TMEM175 does not lead to hyper-acidification in U2OS cells (Fig. 7 B). Treatment with apilimod led to hyper-acidification in both HEK293T (by 0.2 U, pH 5.05 ± 0.06 without treatment and pH 4.85 ± 0.08 with, Fig. 7 A) and U2OS (by 0.49 U, pH 4.57 ± 0.03 without treatment and pH 4.08 ± 0.02 with, Fig. 7 B). KO of TMEM175 did not enhance apilimod-induced hyper-acidification in HEK293T cells (0.19 pH units, pH 5.02 ± 0.07 with treatment and pH 4.83 ± 0.05 without) or U2OS cells (0.36 pH units, pH 4.16 ± 0.03 with treatment and pH 4.52 ± 0.03 without). Thus, TMEM175 does not prevent lysosomal hyper-acidification and lack of TMEM175 does not lead to increased hyper-acidification, strongly arguing against a role as a proton leak channel.

AKT activates lysosomal TMEM175

In previous experiments with pipette solutions of pH 5.5, we found that AKT and its activator SC79 activate TMEM175 (Wie et al., 2021). The role of AKT was challenged by Hu et al., who concluded that AKT is not required for and does not activate TMEM175 (Hu et al., 2022). We further tested the AKT activation using a pH 4.6 pipette solution. In lysosomes dissected from nutrient-replete cells, SC79 increased the outward TMEM175 current by approximately twofold (Fig. 8 A), without much effect on the reversal potential (−26.8 ± 2.1 with SC79 vs −26.2 ± 1.7 mV without). In lysosomes from starved cells, there was little current, but SC79 drastically increased the currents by approximately fourfold (Fig. 8 B). These findings are similar to our previous findings with pH 5.5 pipette solutions and again support the role of AKT in TMEM175 function.

Discussion

Because of the critical role of TMEM175 in PD and its promise as a drug target for Parkinson's therapy, it is essential to understand its contribution to lysosomal physiology. Given the recent contrasting results concerning TMEM175's ion selectivity, we set out to definitively determine the ion selectivity properties of the channel and to further probe its role in lysosomal physiology. We demonstrate here that in the presence of physiological ion concentrations, lysosomal TMEM175 is clearly a K^+-permeable channel, with no more H^+ selectivity than a canonical cation channel. Our in vivo measurements of lysosomal proton leaks reveal extremely low proton permeabilities, with little or no change upon TMEM175 KO, again inconsistent with a primary role in lysosomal proton homeostasis. Finally, though we demonstrate manipulations that can hyper-acidify lysosomes, we do not observe hyper-acidification upon TMEM175 KO in the cells we tested, further evidence to reject the proton conduction hypothesis.

The major point of controversy is on the selectivity of the TMEM175 channel. Hu et al. reported high selectivity for protons in bionic conditions using TMEM175 mistargeted to the plasma membrane. However, all of their critical experiments were carried out in solutions in which protons were the only charge carrier, at least on one side of the membrane. Many cation channels have been shown to change selectivity when their preferred ion is removed completely. For example, the highly

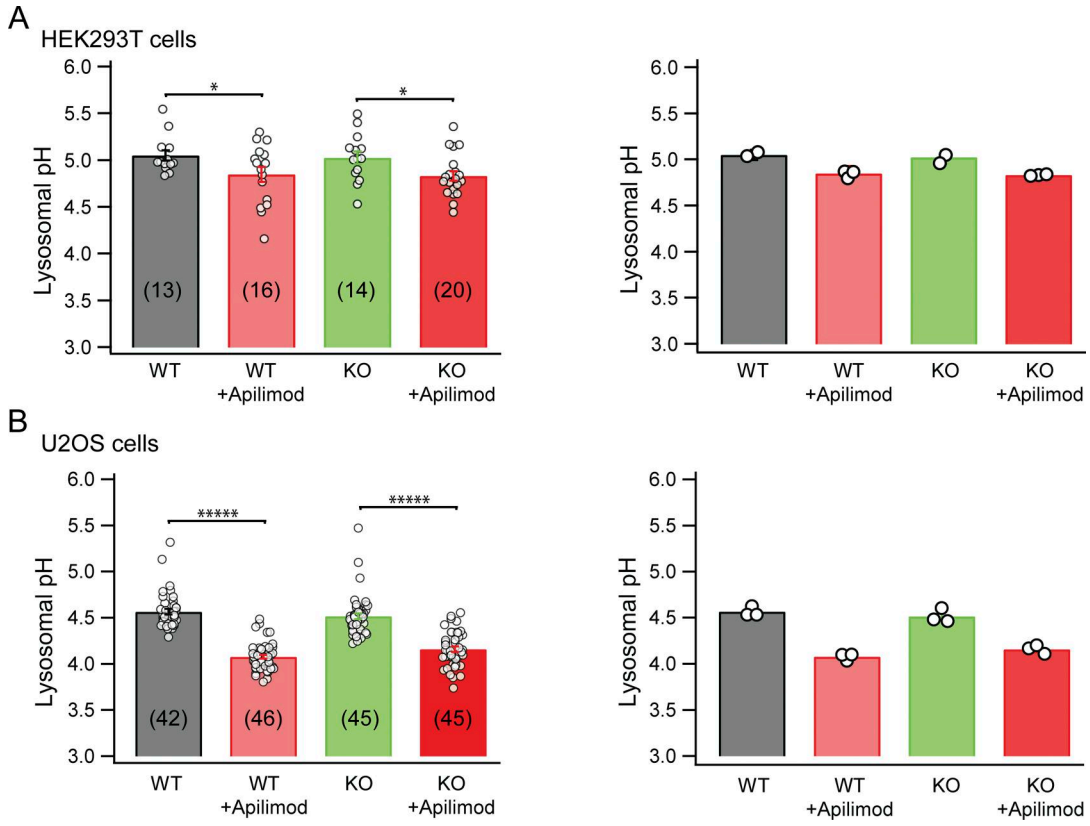

Figure 7. **Lysosomes can be over-acidified in the presence or absence of TMEM175. (A)** Summary of lysosomal pH of WT and TMEM175 KO HEK293T cells with or without apilimod treatment (200 nM, 1 h). Left: Lysosomal pH averaged by cell. The numbers in parenthesis are the number of cells in each condition with each circle representing one cell. Right: Lysosomal pH averaged by independent cell plating and OG loading preparations. Each circle represents one preparation in each respective condition. For HEK293T KO, line TMEM175 KO/5 (Fig. S5) was used. No significant difference in lysosomal pH between WT and KO untreated cells was found, P = 0.78. **(B)** Summary of lysosomal pH of WT and TMEM175 KO U2OS cells with or without apilimod treatment (100 nM, 2 h). Left: Lysosomal pH averaged by cell. The numbers in parenthesis are the number of cells in each condition; each circle represents one cell. Right: Lysosomal pH averaged by experiment; each circle represents one experiment in each respective condition. No significant difference in lysosomal pH between WT and KO untreated cells was found, P = 0.27. P values are from unpaired two-tailed *t* test, where * is P < 0.05 and ***** is P < 10^{-7}. Error bars are SEM.

Ca^{2+}-selective Ca_V channels become nonselective in the absence of extracellular divalent ions Ca^{2+} and Mg^{2+} (Almers and McCleskey, 1984; Hess and Tsien, 1984). Several well-known K^+ channels themselves have been shown to become defunct with impaired conductivity or lose selectivity in the absence of extracellular K^+ (Almers and Armstrong, 1980; Eisenman et al., 1986; Hoshi and Armstrong, 2013; Korn and Ikeda, 1995; Ma et al., 2011; Pardo et al., 1992; Shin et al., 2005; Starkus et al., 1997; Wang et al., 2019; Ye et al., 2010). Indeed, important structural alterations can occur in such circumstances to mediate such changes (Zhou et al., 2001). Here, although we reproduce the finding of proton conduction in plasma membrane–expressed TMEM175 in the nonphysiological condition when other cations are completely depleted, we also observe that even small amounts of potassium reintroduced to the solution can restore the baseline ion preference of the channel.

We further explored TMEM175 proton selectivity in its native environment, lysosomes. In patch-clamp measurements on isolated lysosomes, even in the absence of other cations in the lysosome lumen and at lysosomal pH, we observe only small putative proton currents and then only at relatively high negative voltages (Fig. 2 B). These currents were suppressed by the addition of 150 mM K^+ to the cytosol-equivalent side of the membrane, suggesting that occupancy of the TMEM175 pore by K^+ ions from that side might be sufficient to prevent at least some proton conduction. The gold standard of selectivity determination is the measurement of reversal potentials, which reflect the equilibrium ion preferences of an ion channel system. For lysosomal TMEM175, we consistently measure reversal potentials close to the equilibrium potential for K^+ and far from that of protons. At face value, these values reflect a strong potassium selectivity, a conclusion confirmed by the GHK equation–based estimates of P_H/P_K of 137 or 197 with 0 or 50 mM luminal K^+, respectively. These values are orders of magnitude lower than those of well-characterized H^+ channels like OTOP ($P_H/P_K > 10^5$) or H_V1 ($P_H/P_{Na} > 10^6$) but are comparable to the permeability ratios for canonical channels. Though a permeability ratio of >100 seems high, at a pH of 4.5, $[H^+]$ is ~32 µM, so at 50 mM, potassium is in excess of protons by a factor of about 1,500, suggesting that minimal protons will permeate the channel. Thus, TMEM175 in its physiological environment, lysosomes, is not a H^+-selective channel but is, rather, a K^+ channel, although, like any other K^+ channel, the K^+ flux through the channel may be low when the membrane potential approaches the

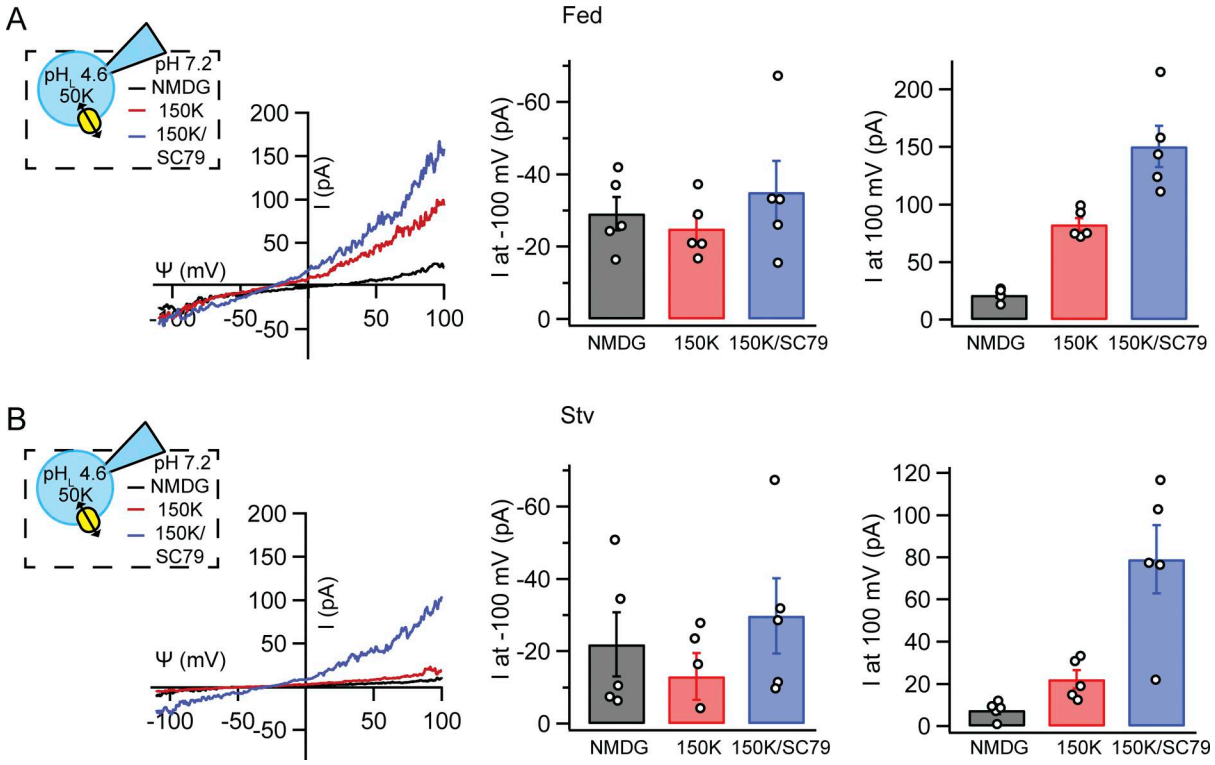

Figure 8. **AKT activates lysosomal TMEM175. (A and B)** Lysosomal currents were recorded from TMEM175-transfected HEK293T cells with (B) or without (A) starvation with pipette solution containing 50 mM K^+, pH 4.6. Left: Representative *I*-Ψ relationships of currents recorded from the same lysosome with bath containing 0 mM K^+ (NMDG), 150 mM K^+, or 150 mM K^+ together with SC79, an AKT activator (10 μM). Middle and right panels: Summary of the inward (at −100 mV) and outward (at +100 mV) current amplitudes. Numbers of lysosomal patches in both fed (A) and starved (B) are n = 5. Error bars are SEM.

equilibrium (Nernst) potential of K^+. The conclusion by Hu et al. that a proton carries >90% of the TMEM175-mediated current at −110–0 mV might be the results of TMEM175 mistargeted to the plasma membrane, where the P_H/P_K is artificially high, recording isolate H^+ currents without physiological K^+, and comparison between lysosomes with artificially large H^+ currents and unrepresentative low K^+ currents.

We used a combination of pH imaging and V-ATPase inhibition to estimate the baseline level of H^+ leak for lysosomes in living cells. The H^+ leaks we measured from neurons and macrophages are extremely small and are within the range of those measured in other cell types by previous investigators. With only one major assumption required (300 nm diameter of lysosomes), our measurements suggest that I_H is only ∼0.02 fA, corresponding to about ∼100 ions/sec and a total H^+ conductance of 0.1 fS (assuming membrane potential of −20 mV and H^+ Nernst potential of +160 mV [Koivusalo et al., 2011]). On the other hand, the endogenous lysosomal K^+ conductance, almost exclusively contributed by TMEM175, is remarkably larger. With 150 mM symmetrical [K^+] and lumen pH of 4.5 or 5.5, the K^+ currents at +100 mV from enlarged lysosomes are ∼20–50 pA (Cang et al., 2015; Wie et al., 2021; Cang et al., 2014), corresponding to a K^+ conductance of ∼200–500 pS. The measurements suggest that the K^+ conductances of native lysosome are ∼2–5 pS (assuming that the lysosomal enlargement used for patch-clamp recording increased the diameter by 10 times and conductance by ∼100 times), 20,000–50,000 times higher than the total H^+ conductance (Fig. 4). Using similar pH imaging methods, Johnson et al. (2016) also reported a low H^+-leak rate of ∼0.4 mM/min in HeLa cells, corresponding to an I_H of 0.009 fA and 57 protons/s (assuming 300 nm lysosomal diameter); both of these values are 10,000–100,000-fold smaller than the 0.1–1 pA of I_H Hu et al. (2022) estimated from the same data. These small leaks are comparable with the rates of proton delivery by the V-ATPase (Maxson et al., 2022), consistent with the idea that at steady state a lysosome pH would be maintained by a balance of proton pumping and proton leak. A proton channel, in contrast, would dramatically destabilize the situation. We do not know the single-channel proton conductance of TMEM175, but if we assume it is comparable with that estimated for Hv1 at pH 5.0, we obtain a value of about 375 fS (Cherny et al., 2003). Even at a very low driving force of 10 mV, the proton flux through a single such channel would be ∼23,000 protons/s, nearly 200-fold larger than we measure for an entire native lysosome. If the turnover rate of the V-ATPase is 300 H^+/sec, then offsetting this leak would require >75 V-ATPases in each lysosome, many more than the 1–2 estimated. Lacking a high density of proton pumps, such rates would rapidly dissipate the entire lysosomal proton gradient.

What are the sources of the small H^+ leak in lysosomes? TMEM175 does not make a significant contribution as knocking it out leads to no significant reduction in the leak. We demonstrated that TRPML1 is also a candidate since it is also H^+-permeable, perhaps more than TMEM175. Like that from TMEM175,

I_H from TRPML1 is also suppressed by K^+ (Fig. 3, B and C), so it is difficult to estimate the channel's contribution to the physiological leak. ClC-7, a lysosomal proton/Cl^- antiporter, could also contribute to the proton leak as it uses protons exiting the lysosome to drive Cl^- into the organelle (Graves et al., 2008; Weinert et al., 2010). Similarly, many of the transporters used to export lysosomal metabolites are proton coupled, using proton exit to drive the export of their nutrient substrates (Kalatzis et al., 2001). However, our measured H^+ permeability of the lysosome (~3×10^{-5} cm/s) is not much higher than that of bare lipid bilayers, which have a H^+ permeability of ~$1–10 \times 10^{-5}$ cm/s (Deamer, 1987). Therefore, a major H^+ permeability from ion channels including TMEM175 and TRPML1 is not expected in baseline conditions.

If the lysosome carries a high-conductance proton channel activated at and essential for normal lysosomal pH, then loss of that activity should lead to significant lysosomal hyper-acidification. Biophysical predictions suggest that the V-ATPase is not at its thermodynamic equilibrium and, if unrestricted by self-regulation or counterion requirements, should be able to acidify the lysosome lumen to nearly pH ~4 (Casey et al., 2010; Grabe et al., 2000). Indeed, recent work reported that fully activating the ClC-7 antiporter in HAP-1 cells hyper-acidifies the organelle to about pH 4.1, among the lowest reported values in mammalian cells (Cao et al., 2023). We found no hyper-acidification in the HEK293T and U2OS TMEM175 KO lines (Figs. 6 and 7), arguing strongly against a role as a pH limiting leak, given that the protein is ubiquitously and constitutively expressed (Cang et al., 2015), and a lack of major H^+-leak channel would lead to hyper-acidification. Hyper-acidification has been reported in some TMEM175 KO cell lines and can be explained by changes in membrane potential (see below; Cang et al., 2015; Jinn et al., 2017; Zhang et al., 2023). However, for the TMEM175 H^+-leak model to hold, it would need to predict hyper-acidification behavior in any cell expressing the protein when TMEM175 is knocked out. In fact, all the KO lysosomes tested are significantly hypo-acidified up to 0.5 pH units when under starvation challenge, during which there is likely a higher demand for K^+ counterion flux. Notably, if, instead, TMEM175 is a K^+ channel that contributes to the counterion pathway and/or regulates lysosomal membrane potential, then loss of function could potentially lead to pH increase, decrease, or no change.

How do ion channels regulate resting pH without conducting H^+ leak? In addition to contributing counterion conductance, ion channels can also regulate lysosomal pH via their contribution to the membrane potential (Ψ), the driving force for the V-ATPase and its "setting point". Together with the pH gradient (ΔpH) between lumen and cytosol, Ψ determines the proton motive force ($pmf = -F.\ \Psi + 2.3\ RT.\ \Delta pH$, where F, R, and T are the Faraday constant, gas constant and temperature in Kelvin, respectively; Ψ is defined with the lumen as "ground" [Bertl et al., 1992]), which in turn determines the driving force for the V-ATPase ($= \Delta G^{o}_{ATP} - N.\ pmf$, where ΔG^{o}_{ATP} is the ATP hydrolysis energy, ~58 kJ/mol; N the H^+/ATP coupling efficiency, not well defined for the lysosomal V-ATPase, possibly 2–4 [Casey et al., 2010]). For an N of 3 and Ψ of 0 mV (Abbas et al., 2020), the thermodynamic equilibrium luminal pH (when $\Delta G^{o}_{ATP} - N.\ pmf = 0$) that the V-ATPase can possibly pump against is 3.9 (assuming cytosolic pH of 7.2), pH 4.2 if $\Psi = -20$ mV (lumen positive [Koivusalo et al., 2011]), and pH 3.6 if Ψ is depolarized to +20 mV (lumen negative). In a TMEM175 KO stable RAW cell line, we indeed found that Ψ is apparently depolarized by ~14 mV compared with WT (Cang et al., 2015), which is equivalent to 0.25 U of pH in the contribution to *pmf*. Intriguingly, ~0.2–0.3 U of hyper-acidification were observed in the several KO stable cell lines by us and others when cells are not starved (Cang et al., 2015; Hu et al., 2022; Jinn et al., 2017). Ψ depolarization–mediated influence on V-ATPase can also explain the ~0.2–0.3 U hyper-acidification found in the mutant mouse lines and human cells that have increased Cl^- influx (CLC-7 gain-of-function mutants [Leray et al., 2022; Nicoli et al., 2019] or increased Na^+ efflux (TPC2 gain-of-function mutant [Wang et al., 2023]). The effect of depolarizing Ψ found in nutrient-replete TMEM175 KO lysosomes is not expected to lead to hyper-acidification in starvation conditions, under which increased H^+ pumping can transiently drive Ψ to negative (lumen more positive) values below both Ψ_K (the Nernst potential for K^+) and Ψ_{Na} such that both Na^+ and K^+ exit the lumen and provide counterion efflux. Indeed, in all the TMEM175 KO cell lines and mouse lines, we found hypo-acidification in mutant lysosomes when the cells are under starvation challenge (Figs. 5 and 6; Cang et al., 2015; Wie et al., 2021).

As we observed in HEK293T and U2OS cell lines, we found no hyper-acidification in hippocampal neurons and macrophages cultured from KO animals under nutrient-replete conditions (Figs. 5 and 6, and [Wie et al., 2021]), again inconsistent with the model of TMEM175 being a H^+-leak channel. In contrast, Hu et al. reported hyper-acidifications in their KO mouse hippocampal neurons. The difference between ours and that of Hu et al. is difficult to reconcile. In our experiments, we used two independent lines that were derived from two founders and have been separately backcrossed for 10 or more generations in >8 years. In addition, WT from the same litter was used as controls. These measures provide the best possible control.

A final prediction of the model is that if TMEM175 is indeed a proton channel, it should dominate all other sources of proton leak—in this case, activating an alternative pathway should minimally affect the lysosomal pH. We tested this model using the drug apilimod, which inhibits synthesis of the lysosomal signaling lipid $PI(3,5)P_2$ and causes depletion of the lipid on the lysosome surface. Apilimod causes lysosomal hyper-acidification by relieving the tonic inhibition of ClC-7 by $PI(3,5)P_2$ (Leray et al., 2022), already indicating that no dominant proton conductance is present. This might be explained if a proton channel was present but with very small conductance, comparable with that of the activated ClC-7. However, in this case, knocking out the TMEM175 proton conductance should enhance the effect of apilimod, an effect not seen in our experiments. Thus, experimental manipulations of lysosomal pH are also inconsistent with TMEM175 functioning as a proton channel under normal conditions.

Lysosomes also communicate with extracellular cues. Using lysosomal recording with pipette (lumen) solutions of pH 5.5, we previously found that both native TMEM175 from neurons and

heterologously expressed TMEM175 in HEK293T cells are activated by extracellular growth factors via AKT. The evidence supporting the role of AKT also includes (1) knocking down AKT or reducing AKT activity by starvation or by allosteric inhibitors all drastically reducing TMEM175 currents and, for starvation, the currents can be restored with the SC79 AKT activator; (2) functional reconstitution of the human TMEM175 in the Drosophila S2 cells also requires a co-expression of human AKT. We have now retested the function of AKT using pipette solutions of pH 4.6 and confirmed the function of AKT (Fig. 8). Our results contradict those by Hu et al. (2022) who concluded that AKT is not required for and does not activate TMEM175 (Hu et al., 2022). The conclusion by Hu et al. that AKT is not required for TMEM175 function is based on their finding that when AKT inhibitors were applied, there was no detectable current (compared with the presence of currents without inhibitor), but application of DCPIB, a channel opener, restored currents. These data, although apparently recording from only one cell was included (Fig. S5 B of Hu et al. [2022]), in our opinion, actually support the role of AKT as AKT inhibitors suppressed the currents, similar to our previous findings (Wie et al., 2021). At best, the data suggest that DCPIB, a channel opener with an unknown mechanism, can bypass the AKT inhibition and open the channel that is closed by the inhibitors. However, it provides no evidence against the role of AKT in channel activation. The conclusion by Hu et al. that SC79 does not activate TMEM175 (Fig. S5 A of Hu et al. [2022]) is also questionable. In the experiments, Hu et al. selected lysosomes that had no basal currents, which is atypical in TMEM175-transfected cells (as shown in other figures in the Hu et al. paper and in previously published ones) and found that application of SC79 activated no obvious currents but DCPIB did. The apparent lack of activation could be simply because lysosomes with little (non-detectable) basal current are selected for the tests, making the SC79-activated currents still too small to detect as SC79 activates currents by only approximately twofold in nutrient-replete cells (Wie et al., 2021). Again, the data, at best, suggest that the channel opener DCPIB is more efficient at opening the channel than a physiological activator AKT but are not against the idea that SC79 activates TMEM175. It is common that a channel opener is more efficient than physiological activators.

In summary, we have used a range of methods to carefully evaluate the functional and physiological contributions of TMEM175 to lysosomal pH regulation. Though our electrophysiological experiments suggest proton conduction under highly non-physiological conditions in the absence of K^+, this conduction is largely lost upon addition of even small amounts of K^+. Experiments in live cells also rule out a major contribution from proton leak channels. These findings represent essential advances given the growing importance of TMEM175 as a risk gene for PD and as a therapeutic target for neurodementia (Chia et al., 2021; Jinn et al., 2017; Wie et al., 2021).

Materials and methods

TMEM175 KO mouse lines

Animal use was approved by the University of Pennsylvania Institutional Animal Care and Use Committee. The generation of TMEM175 KO mouse lines using the CRISPR/Cas9 technique with two guide RNAs targeting exons 3 and 4 (partial sequence in Fig. 5 legend) was previously described (Wie et al., 2021). The 3 independent lines used in the study were from 3 F0 founders and had been backcrossed to C57BL/6J (RRID:IMSR_JAX:000664; Jax lab) for 10 or more generations.

Generation of TMEM175 KO HEK293T cell lines

TMEM175 KO HEK293T cell lines were generated using the CRISPR/Cas9 technique as previously described (Cang et al., 2015). HEK293T cells were infected with CRISPR/Cas9 lentivirus targeting 5′-GCAGGCACTGGATACACCGG[GGG-3′] ([GGG] the PAM sequence). Infected cells were replated and selected with puromycin (3 µg/ml). Single clones were expanded, and DNA amplified from cell lysates using PCR (first PCR: forward primer sequence 5′-AGGCTGCATGGCCGACCTCCAGGAG-3′, reverse primer sequence 5′-ATGATGGACAGCAGGGCGTCA CTG-3′; nested PCR: forward primer sequence.

5′-TTGAATTCACAGGCACACTCAGACCTGCCTTTC-3′, reverse primer sequence 5′-TTGGTACCATGATGGACAGCAGGG CGTCACTG-3′). The primer used to sequence the purified PCR products using Sanger sequencing had a sequence of 5′-TTGGTA CCATGATGGACAGCAGGGCGTCACTG-3′. For cell clones that have mixed alleles, the PCR products were cloned into the EcoRI/KpnI sites of pBluescript II SK(–) and plasmid DNAs were sequenced to determine the genetic disruption.

Cell lines and primary cell cultures

Mammalian cells were maintained at 37°C and 5% CO_2. HEK293T (from RRID:CVCL_0063; ATCC) was authenticated by the providers and was not further authenticated. Cells were cultured in DMEM (Gibco), supplemented with 10% FBS (R&D Systems) and 1× penicillin-streptomycin (Gibco). For neuronal culture, hippocampal and midbrain were dissociated from mouse brains at postnatal day 0 and digested with filtered papain solution (Worthington) for 25–30 min at 37°C. Neurons were dissociated by trituration and plated on 12-mm poly-L-lysine–coated coverslips in 24-well plates. The starting medium (DIV 0) contained 80% DMEM (BioWhittaker with 4.5 g/Liter glucose, 25 mM HEPES, no glutamine), 10% Ham's F-12 (BioWhittaker), 10% bovine calf serum (Hyclone), and 0.5× penicillin-streptomycin. Cells were changed the next day (DIV 1) to Neurobasal A Medium (Gibco) supplemented with 2% B-27 (GIBCO), 0.5× penicillin-streptomycin, 1× GlutaMAX (Gibco), and 25 µM L-glutamate. The following day (DIV 2), media was replaced with Neurobasal A Medium supplemented with 2% B-27, 0.5× penicillin-streptomycin, and 1× GlutaMAX. When necessary, cytosine arabinofuranoside (Sigma-Aldrich) was added at 1 µM to suppress glial growth which was removed before imaging experiments. Hippocampal neurons were imaged on average ∼DIV 8 and midbrain neurons on average ∼DIV 10. For macrophage culture, 10 ml of ice-cold, filtered PBS was injected into the peritoneal cavity of a euthanized adult mouse and extracted after 5 min. Cells were spun down at 1,100 rpm for 10 min. The cell pellet was resuspended in media (DMEM, supplemented with 20% FBS, and 1× penicillin-streptomycin) and plated on either 12- or 25-mm poly-L-lysine-coated coverslips in 6-well plates.

After an hour, the media were replaced with fresh to get rid of nonattached cells. Macrophages were cultured and used for lysosomal pH imaging from DIV 1–4. All primary cells were cultured in WT and TMEM175 KO littermate pairs. Starvation conditions are as follows unless otherwise stated: for HEK293T cells, 2 h of HBSS incubation (Gibco); for neurons, overnight incubation in media without B-27 supplement; and for macrophages, 2 h in buffer containing (in mM) 110 NaCl, 45 $NaHCO_3$, 5 KCl, 2 $CaCl_2$, and 1 $MgCl_2$, pH 7.4 (Cang et al., 2013).

Plasmid DNA constructs and transfections

For HEK293T cell expression, the human TMEM175 used has been previously described (Cang et al., 2015). YFP is attached at the N terminus of human TMEM175 for identification of transfected cells and lysosomes in patch-clamp recordings. The human TRPML1 is GFP tagged and was previously described (Cang et al., 2013). HEK293T cells were transfected using PolyJet (SignaGen) transfection reagent. Transfected cells were replated on 12-mm poly-L-lysine–coated coverslips for electrophysiological experiments around 40 h after transfection for TMEM175 whole cell experiments, 32–40 h for TMEM175 lysosome experiments, and 8 h after transfection for TRPML1 lysosome experiments.

Electrophysiology

All experiments were performed at room temperature (~21°C).

Whole cell patch-clamp recordings

The pipette solution contained (in mM): 150 K-methanesulfonate, 10 TEA chloride, and 20 HEPES, pH 7.2 with KOH (~295 mOsmol/l). Bath solutions with varying [K^+] contained (in mM): K^+ as indicated with additional NMDG to substitute the same amount of K^+ if [K^+] is <50 mM, 100 mM NMDG, 10 Cl^- and either 20 HEPES for pH 7.2 or 20 MES for pH 4.5, pH adjusted with methanesulfonic acid (MSA; ~320 mOsmol/l). Glass pipettes had a resistance of 2–5 MΩ. Only recordings with stable E_{rev} in pH 4.5 NMDG-containing bath were included in our analysis. In cells with multiple paired pH 4.5 NMDG-containing baths and pH 4.5 with varying [K^+] bath exposures, recordings with over 10 mV change in E_{rev} between two recordings with pH 4.5 baths were excluded in our analysis.

Whole organelle patch-clamp recordings from lysosomes

Lysosomes were enlarged with vacuolin-1 (Cayman Chemical Company) treatment and recordings performed as previously described (Cang et al., 2015; Cang et al., 2013; Wie et al., 2021). Each lysosome selected for recording was dissected out of the cell using a glass pipette. Recordings were carried out using a ramp protocol every 10 s (–120–120 mV, in 1 s, Ψ holding at 0 mV, before liquid junction potential [LJP] correction). Ψ is the voltage across the lysosomal membrane with the lumen as the reference ($\Psi = V_{cytosol} - V_{lumen}$; Fig. 2 A; Bertl et al., 1992; note that the definition of Ψ is opposite to what is used in some literatures where cytosol is used as the reference). Outward K^+ current is the movement of K^+ from the cytosol into the lumen, while H^+ leaving the lumen into the cytosol is inward current. Pipette solutions with 0 mM K^+ contained (in mM) 20 MES, 150 NMDG, and 2 Cl^-, pH 4.6 or 4.0, with MSA. Pipette solutions containing 5 mM or 50 mM K^+ had the same composition as 0 mM K^+ pipette except for a corresponding decrease in [NMDG] with the respective [K^+] (~300 mOsmol/l). Bath solutions with or without K^+ contained (in mM): 20 HEPES, 150 K^+ (or replaced with 150 NMDG in 0 mM K^+ bath), and 2 Cl^-, pH 7.2, with MSA (~305 mOsm/l). For TRPML1 recordings, 1 μM of $PI(3,5)P_2$, when indicated, was added from a 1 mM stock of water-soluble diC8 form (Echelon Biosciences; 0.1% of total bath volume). For TMEM175 recordings with SC79 (Calbiochem), 10 μM was added to the bath (final DMSO concentration of 0.1%).

Recordings were performed with a MultiClamp 700B Microelectrode Amplifier and a Digidata 1440A controlled with pClamp and Clampfit (version 10.4; Molecular Devices), used for data collection and processing. LJPs were calculated in pClamp and corrected offline for E_{rev} and Ψ_{rev} determination. All recordings were from at least two batches of transfected HEK293T cells.

TMEM175 currents were generally smaller when recorded K^+ bath and pipette solutions with pH 4.6 or pH 4.0 than those recorded with pH 5.5 pipette solution (Cang et al., 2015; Wie et al., 2021), presumably because of inhibition of K^+ conductance by H^+, as found in plasma membrane–targeted TMEM175 (Zheng et al., 2022). To minimize contamination by nonspecific leak for the estimation of reversal potentials, we applied offline leak subtraction when recordings with an NMDG bath (no K^+, pH 7.2) had outward currents (at +100 mV, before liquid junction correction) >10 pA for lysosomal recording or inward currents at –100 mV >20 pA. These currents recorded from NMDG-containing baths were considered to be largely from nonspecific leak. Recordings were filtered at 100 Hz. The traces in pH 7.2 NMDG bath were used to obtain a leak conductance by fitting the current in the voltage range between 95 mV and 100 mV for lysosomal recordings, or –100 to –95 mV for whole cell recordings, to the equation of $i = G_L \Psi$ (or V for whole cell, i intercept at 0 mV). For lysosomal recording, we assume that there is little outward H^+ current (H^+ moving into the lumen) at –100 mV when recorded with pH 7.2 containing NMDG bath because of the low [H^+]. In case there is a small trace H^+ inward current, the currents would have been under-subtracted, resulting in an underestimate of Ψ_{rev} obtained in 150 mM K^+ bath toward 0 mV and an over-estimate of P_H/P_K, which would not affect our conclusion that TMEM175 is not a H^+-selective channel. Linear leak subtraction was applied to qualified recordings from lysosomes (Figs. 2 and 3) and whole cell (Fig. 1), but not the lysosomal TMEM175 recordings in Fig. 8 for a more accurate comparison between the fed and starved states, since the recordings in pH 7.2 containing NMDG bath after starvation were predominantly under 10 pA at 100 mV and therefore had no leak subtraction applied. For Ψ_{rev} determination in whole lysosome experiments, only recordings with currents (inward or outward) >20 pA (after leak subtraction) were selected to minimize random errors in recordings of small sizes.

LJP-corrected E_{rev} and Ψ_{rev} averages for each condition were used to calculate the P_H/P_K using the equation below, where R, T, and F are the gas constant, absolute temperature, Faraday's

constant, respectively. $[K]_i$ and $[H]_i$ refer to the internal concentrations of each ion (pipette concentrations for whole cell and bath for whole lysosome recordings), while $[K]_o$ and $[H]_o$ are the external concentrations of each ion (bath concentration for whole cell and pipette solutions for whole lysosome recordings).

$$\frac{P_H}{P_K} = \frac{e^{\left(\frac{Erev*F}{RT}\right)}[K]_i - [K]_o}{[H]_o - e^{\left(\frac{Erev*F}{RT}\right)}[H]_i}$$

Lysosomal pH imaging

All imaging experiments were performed at room temperature (~21°C).

Determining lysosomal pH

The protocol was adapted from previous studies (Cang et al., 2013; Steinberg et al., 2010). Cells plated on poly-L-lysine–coated coverslips were loaded with OG 10,000 MW dextran (Invitrogen) overnight, 250 µg/ml used for macrophages and HEK293T cells and 150 µg/ml for neurons. Before imaging, macrophages and HEK293T cells were chased in either fresh culture media or, for starvation condition, starvation buffers (see Cell lines and primary cell cultures section for buffer compositions) for 2 h, while neurons were chased for 3 h with fresh culture media with or without (for starvation condition) B-27. Cells were washed with imaging solutions and imaged with an IX71 Olympus microscope using a 60× objective, NA 1.2. Imaging solutions contained (in mM) 140 NaCl, 3.5 KCl, 2 $MgCl_2$, 2 $CaCl_2$, 20 HEPES/NaOH pH 7.4, and 20 glucose for fed conditions (absent in starvation image solutions). The imaging solution for fed neurons also contained 1× amino acid (50× Amino Acid Mixture, Gibco). Fluorescence was excited at 440 and 490 nm with DeltaRAW V monochromator (PTI), emission filtered at 540 ± 25 nm and acquired with an EMCCD camera (Evolve 512; Photometric) controlled with MetaFluor software (Molecular Devices). After collecting images of cells, an in situ pH calibration was performed for each coverslip. Each calibration pH was imaged three times after a 5-min waiting period, from either pH 7 to pH 4 in 0.5 pH increments (with or without pH 6.0) or pH 6.5 to pH 3.5 in 0.5 pH increments. At least 5 different pH solutions were used for the generation of a calibration curve. The calibration solutions consist of (in mM) 140 KCl, 3.5 NaCl, 2 $MgCl_2$, 2 $CaCl_2$, 20 glucose, 20 buffering agents (HEPES for pH 7 and 6.5, MES for pH 6–4.5, acetate/acidic acid for pH 4 and 3.5), and 10 µM nigericin (Sigma-Aldrich). Images were imported into ImageJ for analysis where individual lysosomes were selected as regions of interest along with background regions. The corresponding integrated intensities of the selected lysosomes at both 440 and 490 nm after background subtraction were used to determine the 490/440 nm ratio. The calibration pH's average 490/440 nm ratios were fit to a sigmoid curve. The fit was then used to convert the average 490/440 nm ratios of lysosomes in each cell from the same coverslip to pH values. In neurons, most of the lysosomes analyzed were localized to the soma; HEK293T cell lysosomes were a mixture of perinuclear and peripheral localization; macrophage lysosomes selected for analysis were mainly localized in the cell periphery since perinuclear lysosomes were generally crowded and could not be individually distinguished. Each condition reported contains data from at least two coverslips (each with its own calibration) and, for primary cultures from mice, data from at least two different littermate WT and TMEM175 KO pairs for neurons and macrophages.

Lysosomal pH with apilimod treatment in HEK293T cells

The lysosome pH imaging experiments with apilimod (Chem Cruz) treatment to observe acidification effects were conducted as described above with one difference. The HEK293T cells were chased for 2 h in fresh culture media, then treated with 200 nM apilimod for 1 h in culture media before proceeding with imaging (DMSO final concentration 0.2%). At least two coverslips from different plating and OG-loading preparations were used for WT and TMEM175 KO/5 HEK293T fed conditions and at least three coverslips were used to quantify the lysosomal pH of apilimod treated WT and TMEM175 KO/5 HEK293T cells from at least two independent coverslip plating and OG-loading preparations.

Determining lysosomal pH in U2OS cells

A comprehensive description of the ratiometric pH imaging used for U2OS cells (U-2 OS HTB-96, RRID:CVCL_0042; ATCC) was previously described (Leray et al., 2022). The U2OS KO cell line was generated by Ubigene. Cells were cultured in McCoy's 5A (modified) medium and seeded into 96-well plates the morning before experimentation. For dye loading, cells were treated with a medium containing 1 mg/ml OG. After overnight incubation (~15 h), the cells were washed with dye-free medium. This was followed by a 4-h chase period and a subsequent 2-h treatment with either 100 nM Apilimod or vehicle DMSO. For imaging, the medium was replaced with an imaging solution consisting (in mM) of 150 NaCl, 5 KCl, 1 $MgCl_2$, 1 $CaCl_2$, 10 glucose, 30 sucrose, and 20 HEPES, pH 7.2. Imaging was conducted at room temperature using a Nikon Eclipse Ti microscope equipped with a 60× objective, NAN 1.49 (Apo TIRF, Nikon) and a digital camera (Hamamatsu), with LED excitation at wavelengths of 435 and 490 nm. The pH values were derived from the fluorescence ratios after application of pH calibration buffers ranging from pH 3.5–7.0, which included monensin and nigericin to equilibrate intracellular pH. Image analysis was performed using Slicer2D software (Lau et al., 2013), and data visualization was done using GraphPad Prism version 9.3.1.

H^+-leak measurements

H^+-leak measurement experiments were adopted from a previously described method (Johnson et al., 2016). The cells on poly-L-lysine coverslips were loaded with OG overnight, as described above with the same imaging set up and imaging/calibration solutions (all fed). Three images of the selected cells over the course of 1 min were taken as a baseline before concanamycin A (Chem Cruz) was added. Macrophages had 2 µM added while 5 µM of concanamycin A was added to hippocampal neurons (final DMSO 0.04% and 0.1%, respectively). Images with excitation 440 and 490 nm were collected at intervals of 1 min over 20 min. The weak base ammonium chloride was then added, 5 mM for macrophages and 10 mM for neurons, and cells were imaged for 5 min, followed by an in situ calibration. At least 20 lysosomes were analyzed per cell. The change in pH was

determined by the slope of the line fit to the pH values of the concanamycin A addition time course before ammonium chloride was added. The lysosomes' intralysosomal [$NH4^+$] ([$NH4^+$]$_L$) was calculated using the Henderson–Hasselbalch equation, and the intrinsic buffering capacity (mM/pH) was calculated as $\Delta[NH4^+]_L/\Delta pH_L$ for each cell. The [H^+] decrease (mM/min) was obtained by multiplying the buffering capacity by the overall $\Delta pH/\Delta t$ when exposed to concanamycin A for each cell. We used HeLa cells as a control (2 µM concanamycin A and 3.75 mM ammonium chloride) and obtained parameters comparable with those previously determined by Johnson et al. (2016) (pH change 0.062 ± 0.01 pH/min, buffering capacity 8.9 ± 0.8 mM/pH, and H^+ leak/[H^+] decrease 0.45 ± 0.04 mM/min, n = 4). The pH changes in neuronal lysosomes upon ammonium chloride application were generally slower and smaller than those in macrophages and HeLa cells (RRID: CVCL_0030; ATCC), presumably due to higher buffering capacity in neuronal lysosomes.

LysoTracker staining

Cells plated on 12-mm poly-L-lysine–coated coverslips were treated with 150 nM LysoTracker Red DND-99 (Invitrogen) for 30 min at 37°C and 5% CO_2. The coverslips were washed with the respective imaging solution. The fluorescence excited at 577 nm was collected with a 630 ± 30-nm emission filter. Each coverslip was collected in WT and TMEM175 KO pairs in quick succession so that the conditions could be as similar as possible. The same imaging solutions and starvation conditions as the OG imaging experiments were used. The collected fluorescence images were imported and analyzed in ImageJ where cells (macrophages) and lysosomes (hippocampal neurons) were selected as regions of interest with background subtraction. The integrated fluorescence intensities were normalized to the average of the paired WT coverslips to examine the relative difference in pH between WT and TMEM175 KO.

Quantification and statistical analysis

Clampfit and Excel were used to process electrophysical data. IGOR was used to fit calibration curves for OG lysosomal pH determination and pH change during concanamycin A time course for H^+-leak experiments and to determine the leak line for leak subtraction in electrophysiological experiments. ImageJ was used to select regions of interest and analyze microscopy images which were averaged and normalized when applicable in Excel. For lysosomal pH in U2OS cells, Slicer2D software was used to analyze microscopy images and data visualization was done using GraphPad Prism version 9.3.1. The statistical details can be found in the corresponding figure legends. Data are presented as ± SEM. For statistical analysis, the two-way Student's t test was used to check for significance. Significance is indicated as not significant (ns), *$P < 0.05$, ****$P < 10^{-6}$, and *****$P < 10^{-7}$. Data distribution was assumed to be normal, but this was not formally tested.

Online supplemental material

Fig. S1 shows whole organelle currents of non-transfected lysosomes in the same experimental set up used in Fig. 2. Fig. S2 shows lysosomal currents of TMEM175 with luminal pH of 4.0. Fig. S3 shows TMEM175 KO lysosomal alkalinization using fluorescent dye, LysoTracker. Fig. S4 breaks down the lysosomal pH of WT and TMEM175 KO cells by animal (mouse or KO line). Fig. S5 describes HEK293T TMEM175 KO generated cells.

Data availability

Original traces of electrophysiological recordings and microscope images will be shared by the lead contact upon request. Any additional information required to reanalyze the data reported in the paper is available from the lead contact upon request.

Acknowledgments

The contributions of the National Institutes of Health (NIH) authors, Vedrana Mikusevic and Joseph A. Mindell, were made as part of their official duties as NIH federal employees, are in compliance with agency policy requirements, and are considered Works of the US Government. However, the findings and conclusions presented in this paper are those of the authors and do not necessarily reflect the views of the NIH or the US Department of Health and Human Services. We thank Dr. Chunlei Cang and Dr. Tosh Hoshi for discussions and sharing unpublished results. Dejian Ren received speaking honorarium and licensing fees related to work. Research in this study was supported, in part, by a grant from the National Institute of General Medical Sciences (1 R01 GM133172 to Dejian Ren). Vedrana Mikusevic and Joseph A. Mindell were supported by the National Institute of Neurological Disorders and Stroke intramural program. This research was supported in part by the Intramural Research Program of the NIH.

Author contributions: Erika Riederer: conceptualization, data curation, formal analysis, investigation, methodology, validation, visualization, and writing—original draft, review, and editing. Vedrana Mikusevic: conceptualization, data curation, formal analysis, investigation, methodology, validation, visualization, and writing—original draft. Tuoxian Tang: investigation. Lillian Martin: investigation. Joseph A. Mindell: conceptualization, formal analysis, funding acquisition, methodology, project administration, resources, supervision, and writing—original draft, review, and editing, Dejian Ren: conceptualization, data curation, formal analysis, funding acquisition, investigation, methodology, project administration, resources, supervision, visualization, writing—original draft, review, and editing.

Disclosures: All authors have completed and submitted the ICMJE Form for Disclosure of Potential Conflicts of Interest. D. Ren reported "D. Ren has received speaking honorarium and licensing fees related to work." No other disclosures were reported.

Submitted: 21 January 2025
Revised: 24 September 2025
Accepted: 7 October 2025

References

Abbas, Y.M., D. Wu, S.A. Bueler, C.V. Robinson, and J.L. Rubinstein. 2020. Structure of V-ATPase from the mammalian brain. *Science*. 367: 1240–1246. https://doi.org/10.1126/science.aaz2924

Almers, W., and C.M. Armstrong. 1980. Survival of K^+ permeability and gating currents in squid axons perfused with K^+-free media. *J. Gen. Physiol.* 75:61–78. https://doi.org/10.1085/jgp.75.1.61

Almers, W., and E.W. McCleskey. 1984. Non-selective conductance in calcium channels of frog muscle: Calcium selectivity in a single-file pore. *J. Physiol.* 353:585–608. https://doi.org/10.1113/jphysiol.1984.sp015352

Andrews, N.W. 2000. Regulated secretion of conventional lysosomes. *Trends Cell Biol.* 10:316–321. https://doi.org/10.1016/s0962-8924(00)01794-3

Ballabio, A., and J.S. Bonifacino. 2020. Lysosomes as dynamic regulators of cell and organismal homeostasis. *Nat. Rev. Mol. Cell Biol.* 21:101–118. https://doi.org/10.1038/s41580-019-0185-4

Ballabio, A., and V. Gieselmann. 2009. Lysosomal disorders: From storage to cellular damage. *Biochim. Biophys. Acta*. 1793:684–696. https://doi.org/10.1016/j.bbamcr.2008.12.001

Bertl, A., E. Blumwald, R. Coronado, R. Eisenberg, G. Findlay, D. Gradmann, B. Hille, K. Köhler, H.-A. Kolb, E. MacRobbie, et al. 1992. Electrical measurements on endomembranes. *Science*. 258:873–874. https://doi.org/10.1126/science.1439795

Brunner, J.D., R.P. Jakob, T. Schulze, Y. Neldner, A. Moroni, G. Thiel, T. Maier, and S. Schenck. 2020. Structural basis for ion selectivity in TMEM175 K(+) channels. *Elife*. 9:e53683. https://doi.org/10.7554/eLife.53683

Burbulla, L.F., P. Song, J.R. Mazzulli, E. Zampese, Y.C. Wong, S. Jeon, D.P. Santos, J. Blanz, C.D. Obermaier, C. Strojny, et al. 2017. Dopamine oxidation mediates mitochondrial and lysosomal dysfunction in Parkinson's disease. *Science*. 357:1255–1261. https://doi.org/10.1126/science.aam9080

Cang, C., K. Aranda, Y.-J. Seo, B. Gasnier, and D. Ren. 2015. TMEM175 is an Organelle K(+) channel regulating lysosomal function. *Cell*. 162: 1101–1112. https://doi.org/10.1016/j.cell.2015.08.002

Cang, C., B. Bekele, and D. Ren. 2014. The voltage-gated sodium channel TPC1 confers endolysosomal excitability. *Nat. Chem. Biol.* 10:463–469. https://doi.org/10.1038/nchembio.1522

Cang, C., Y. Zhou, B. Navarro, Y.-J. Seo, K. Aranda, L. Shi, S. Battaglia-Hsu, I. Nissim, D.E. Clapham, and D. Ren. 2013. mTOR regulates lysosomal ATP-sensitive two-pore Na^+ channels to adapt to metabolic state. *Cell*. 152:778–790. https://doi.org/10.1016/j.cell.2013.01.023

Cao, X., G.M. Lenk, V. Mikusevic, J.A. Mindell, and M.H. Meisler. 2023. The chloride antiporter CLCN7 is a modifier of lysosome dysfunction in FIG4 and VAC14 mutants. *Plos Genet.* 19:e1010800. https://doi.org/10.1371/journal.pgen.1010800

Casey, J.R., S. Grinstein, and J. Orlowski. 2010. Sensors and regulators of intracellular pH. *Nat. Rev. Mol. Cell Biol.* 11:50–61. https://doi.org/10.1038/nrm2820

Caterina, M.J., M.A. Schumacher, M. Tominaga, T.A. Rosen, J.D. Levine, and D. Julius. 1997. The capsaicin receptor: A heat-activated ion channel in the pain pathway. *Nature*. 389:816–824. https://doi.org/10.1038/39807

Chang, D., M.A. Nalls, I.B. Hallgrimsdóttir, J. Hunkapiller, M. van der Brug, F. Cai, International Parkinson's Disease Genomics Consortium, 23andMe Research Team, G.A. Kerchner, G. Ayalon, et al. 2017. A meta-analysis of genome-wide association studies identifies 17 new Parkinson's disease risk loci. *Nat. Genet.* 49:1511–1516. https://doi.org/10.1038/ng.3955

Chapel, A., S. Kieffer-Jaquinod, C. Sagné, Q. Verdon, C. Ivaldi, M. Mellal, J. Thirion, M. Jadot, C. Bruley, J. Garin, et al. 2013. An extended proteome map of the lysosomal membrane reveals novel potential transporters. *Mol. Cell. Proteomics* 12:1572–1588. https://doi.org/10.1074/mcp.M112.021980

Cherny, V.V., R. Murphy, V. Sokolov, R.A. Levis, and T.E. DeCoursey. 2003. Properties of single voltage-gated proton channels in human eosinophils estimated by noise analysis and by direct measurement. *J. Gen. Physiol.* 121:615–628. https://doi.org/10.1085/jgp.200308813

Chia, R., M.S. Sabir, S. Bandres-Ciga, S. Saez-Atienzar, R.H. Reynolds, E. Gustavsson, R.L. Walton, S. Ahmed, C. Viollet, J. Ding, et al. 2021. Genome sequencing analysis identifies new loci associated with lewy body dementia and provides insights into its genetic architecture. *Nat. Genet.* 53:294–303. https://doi.org/10.1038/s41588-021-00785-3

Cuppoletti, J., D. Aures-Fischer, and G. Sachs. 1987. The lysosomal H^+ pump: 8-azido-ATP inhibition and the role of chloride in H^+ transport. *Biochim. Biophys. Acta*. 899:276–284. https://doi.org/10.1016/0005-2736(87)90409-3

Deamer, D.W. 1987. Proton permeation of lipid bilayers. *J. Bioenerg. Biomembr.* 19:457–479. https://doi.org/10.1007/BF00770030

Decoursey, T.E. 2003. Voltage-gated proton channels and other proton transfer pathways. *Physiol. Rev.* 83:475–579. https://doi.org/10.1152/physrev.00028.2002

DiCiccio, J.E., and B.E. Steinberg. 2011. Lysosomal pH and analysis of the counter ion pathways that support acidification. *J. Gen. Physiol.* 137: 385–390. https://doi.org/10.1085/jgp.201110596

Dong, X.P., D. Shen, X. Wang, T. Dawson, X. Li, Q. Zhang, X. Cheng, Y. Zhang, L.S. Weisman, M. Delling, and H. Xu. 2010. PI(3,5)P(2) controls membrane trafficking by direct activation of mucolipin Ca^{2+} release channels in the endolysosome. *Nat. Commun.* 1:38. https://doi.org/10.1038/ncomms1037

Eisenman, G., R. Latorre, and C. Miller. 1986. Multi-ion conduction and selectivity in the high-conductance Ca^{++}-activated K^+ channel from skeletal muscle. *Biophys. J.* 50:1025–1034. https://doi.org/10.1016/S0006-3495(86)83546-9

Galione, A., J. Parrington, and T. Funnell. 2011. Physiological roles of NAADP-mediated Ca^{2+} signaling. *Sci. China. Life Sci.* 54:725–732. https://doi.org/10.1007/s11427-011-4207-5

Goul, C., R. Peruzzo, and R. Zoncu. 2023. The molecular basis of nutrient sensing and signalling by mTORC1 in metabolism regulation and disease. *Nat. Rev. Mol. Cell Biol.* 24:857–875. https://doi.org/10.1038/s41580-023-00641-8

Grabe, M., H. Wang, and G. Oster. 2000. The mechanochemistry of V-ATPase proton pumps. *Biophys. J.* 78:2798–2813. https://doi.org/10.1016/S0006-3495(00)76823-8

Graves, A.R., P.K. Curran, C.L. Smith, and J.A. Mindell. 2008. The Cl^-/H^+ antiporter ClC-7 is the primary chloride permeation pathway in lysosomes. *Nature*. 453:788–792. https://doi.org/10.1038/nature06907

Harikumar, P., and J.P. Reeves. 1983. The lysosomal proton pump is electrogenic. *J. Biol. Chem.* 258:10403–10410.

Hellwig, N., T.D. Plant, W. Janson, M. Schäfer, G. Schultz, and M. Schaefer. 2004. TRPV1 acts as proton channel to induce acidification in nociceptive neurons. *J. Biol. Chem.* 279:34553–34561. https://doi.org/10.1074/jbc.M402966200

Hess, P., and R.W. Tsien. 1984. Mechanism of ion permeation through calcium channels. *Nature*. 309:453–456. https://doi.org/10.1038/309453a0

Hoshi, T., and C.M. Armstrong. 2013. C-type inactivation of voltage-gated K^+ channels: Pore constriction or dilation? *J. Gen. Physiol.* 141:151–160. https://doi.org/10.1085/jgp.201210888

Hu, M., P. Li, C. Wang, X. Feng, Q. Geng, W. Chen, M. Marthi, W. Zhang, C. Gao, W. Reid, et al. 2022. Parkinson's disease-risk protein TMEM175 is a proton-activated proton channel in lysosomes. *Cell*. 185:2292–2308.e20. https://doi.org/10.1016/j.cell.2022.05.021

Jiang, J., M. Li, and L. Yue. 2005. Potentiation of TRPM7 inward currents by protons. *J. Gen. Physiol.* 126:137–150. https://doi.org/10.1085/jgp.200409185

Jinn, S., R.E. Drolet, P.E. Cramer, A.H.-K. Wong, D.M. Toolan, C.A. Gretzula, B. Voleti, G. Vassileva, J. Disa, M. Tadin-Strapps, and D.J. Stone. 2017. TMEM175 deficiency impairs lysosomal and mitochondrial function and increases alpha-synuclein aggregation. *Proc. Natl. Acad. Sci. USA*. 114: 2389–2394. https://doi.org/10.1073/pnas.1616332114

Johnson, D.E., P. Ostrowski, V. Jaumouillé, and S. Grinstein. 2016. The position of lysosomes within the cell determines their luminal pH. *J. Cell Biol.* 212:677–692. https://doi.org/10.1083/jcb.201507112

Kalatzis, V., S. Cherqui, C. Antignac, and B. Gasnier. 2001. Cystinosin, the protein defective in cystinosis, is a H^+-driven lysosomal cystine transporter. *Embo J.* 20:5940–5949. https://doi.org/10.1093/emboj/20.21.5940

Kaushik, S., and A.M. Cuervo. 2018. The coming of age of chaperone-mediated autophagy. *Nat. Rev. Mol. Cell Biol.* 19:365–381. https://doi.org/10.1038/s41580-018-0001-6

Koivusalo, M., B.E. Steinberg, D. Mason, and S. Grinstein. 2011. In situ measurement of the electrical potential across the lysosomal membrane using FRET. *Traffic*. 12:972–982. https://doi.org/10.1111/j.1600-0854.2011.01215.x

Kolter, T., and K. Sandhoff. 2005. Principles of lysosomal membrane digestion: Stimulation of sphingolipid degradation by sphingolipid activator proteins and anionic lysosomal lipids. *Annu. Rev. Cell Dev. Biol.* 21:81–103. https://doi.org/10.1146/annurev.cellbio.21.122303.120013

Korn, S.J., and S.R. Ikeda. 1995. Permeation selectivity by competition in a delayed rectifier potassium channel. *Science*. 269:410–412. https://doi.org/10.1126/science.7618108

Korolchuk, V.I., S. Saiki, M. Lichtenberg, F.H. Siddiqi, E.A. Roberts, S. Imarisio, L. Jahreiss, S. Sarkar, M. Futter, F.M. Menzies, et al. 2011. Lysosomal positioning coordinates cellular nutrient responses. *Nat. Cell Biol.* 13:453–460. https://doi.org/10.1038/ncb2204

Kosmidis, E., C.G. Shuttle, J. Preobraschenski, M. Ganzella, P.J. Johnson, S. Veshaguri, J. Holmkvist, M.P. Møller, O. Marantos, F. Marcoline, et al. 2022. Regulation of the mammalian-brain V-ATPase through ultraslow mode-switching. *Nature*. 611:827–834. https://doi.org/10.1038/s41586-022-05472-9

Lau, W.W., C.A. Johnson, S. Lioi, and J.A. Mindell. 2013. Three-dimensional spot detection in ratiometric fluorescence imaging for measurement of subcellular organelles. *ACM Conf. Bioinform. Comput. Biol. Biomed. Inform.* 2013:722. https://doi.org/10.1145/2506583.2512387

Lee, C., J. Guo, W. Zeng, S. Kim, J. She, C. Cang, D. Ren, and Y. Jiang. 2017. The lysosomal potassium channel TMEM175 adopts a novel tetrameric architecture. *Nature*. 547:472–475. https://doi.org/10.1038/nature23269

Leray, X., J.K. Hilton, K. Nwangwu, A. Becerril, V. Mikusevic, G. Fitzgerald, A. Amin, M.R. Weston, and J.A. Mindell. 2022. Tonic inhibition of the chloride/proton antiporter ClC-7 by PI(3,5)P2 is crucial for lysosomal pH maintenance. *Elife*. 11:e74136. https://doi.org/10.7554/eLife.74136

Lie, P.P.Y., and R.A. Nixon. 2018. Lysosome trafficking and signaling in health and neurodegenerative diseases. *Neurobiol. Dis.* 122:94–105. https://doi.org/10.1016/j.nbd.2018.05.015

Loboda, A., A. Melishchuk, and C. Armstrong. 2001. Dilated and defunct K channels in the absence of K^+. *Biophys. J.* 80:2704–2714. https://doi.org/10.1016/S0006-3495(01)76239-X

López-Otín, C., M.A. Blasco, L. Partridge, M. Serrano, and G. Kroemer. 2013. The hallmarks of aging. *Cell*. 153:1194–1217. https://doi.org/10.1016/j.cell.2013.05.039

Ma, L., X. Zhang, and H. Chen. 2011. TWIK-1 two-pore domain potassium channels change ion selectivity and conduct inward leak sodium currents in hypokalemia. *Sci. Signal.* 4:ra37. https://doi.org/10.1126/scisignal.2001726

Maxson, M.E., Y.M. Abbas, J.Z. Wu, J.D. Plumb, S. Grinstein, and J.L. Rubinstein. 2022. Detection and quantification of the vacuolar H+ATPase using the legionella effector protein SidK. *J. Cell Biol.* 221:e202107174. https://doi.org/10.1083/jcb.202107174

Mellman, I. 1989. Organelles observed: Lysosomes. *Science*. 244:853–854. https://doi.org/10.1126/science.244.4906.853

Mindell, J.A. 2012. Lysosomal acidification mechanisms. *Annu. Rev. Physiol.* 74:69–86. https://doi.org/10.1146/annurev-physiol-012110-142317

Morgan, A.J., F.M. Platt, E. Lloyd-Evans, and A. Galione. 2011. Molecular mechanisms of endolysosomal Ca^{2+} signalling in health and disease. *Biochem. J.* 439:349–374. https://doi.org/10.1042/BJ20110949

Mozhayeva, G.N., and A.P. Naumov. 1983. The permeability of sodium channels to hydrogen ions in nerve fibres. *Pflugers Arch.* 396:163–173. https://doi.org/10.1007/BF00615521

Nicoli, E.R., M.R. Weston, M. Hackbarth, A. Becerril, A. Larson, W.M. Zein, P.R. Baker 2nd, J.D. Burke, H. Dorward, M. Davids, et al. 2019. Lysosomal Storage and Albinism Due to Effects of a De Novo CLCN7 Variant on Lysosomal Acidification. *Am. J. Hum. Genet.* 104:1127–1138. https://doi.org/10.1016/j.ajhg.2019.04.008

Numata, T., and Y. Okada. 2008. Proton conductivity through the human TRPM7 channel and its molecular determinants. *J. Biol. Chem.* 283:15097–15103. https://doi.org/10.1074/jbc.M709261200

Oh, S., N. Paknejad, and R.K. Hite. 2020. Gating and selectivity mechanisms for the lysosomal K(+) channel TMEM175. *Elife*. 9:e53430. https://doi.org/10.7554/eLife.53430

Ohkuma, S., Y. Moriyama, and T. Takano. 1982. Identification and characterization of a proton pump on lysosomes by fluorescein-isothiocyanate-dextran fluorescence. *Proc. Natl. Acad. Sci. USA*. 79:2758–2762. https://doi.org/10.1073/pnas.79.9.2758

Ohkuma, S., Y. Moriyama, and T. Takano. 1983. Electrogenic nature of lysosomal proton pump as revealed with a cyanine dye. *J. Biochem.* 94:1935–1943. https://doi.org/10.1093/oxfordjournals.jbchem.a134547

Pardo, L.A., S.H. Heinemann, H. Terlau, U. Ludewig, C. Lorra, O. Pongs, and W. Stuhmer. 1992. Extracellular K^+ specifically modulates a rat brain K^+ channel. *Proc. Natl. Acad. Sci. USA*. 89:2466–2470. https://doi.org/10.1073/pnas.89.6.2466

Platt, F.M., B. Boland, and A.C. van der Spoel. 2012. The cell biology of disease: Lysosomal storage disorders: The cellular impact of lysosomal dysfunction. *J. Cell Biol.* 199:723–734. https://doi.org/10.1083/jcb.201208152

Riederer, E., C. Cang, and D. Ren. 2023. Lysosomal ion channels: What are they good for and are they druggable targets? *Annu. Rev. Pharmacol. Toxicol.* 63:19–41. https://doi.org/10.1146/annurev-pharmtox-051921-013755

Rubinsztein, D.C., G. Mariño, and G. Kroemer. 2011. Autophagy and aging. *Cell*. 146:682–695. https://doi.org/10.1016/j.cell.2011.07.030

Saxton, R.A., and D.M. Sabatini. 2017. mTOR signaling in growth, metabolism, and disease. *Cell*. 169:361–371. https://doi.org/10.1016/j.cell.2017.03.035

Schroder, B., C. Wrocklage, C. Pan, R. Jäger, B. Kösters, H. Schäfer, H.P. Elsässer, M. Mann, and A. Hasilik. 2007. Integral and associated lysosomal membrane proteins. *Traffic*. 8:1676–1686. https://doi.org/10.1111/j.1600-0854.2007.00643.x

Settembre, C., and A. Ballabio. 2014. Lysosome: Regulator of lipid degradation pathways. *Trends Cell Biol.* 24:743–750. https://doi.org/10.1016/j.tcb.2014.06.006

Settembre, C., A. Fraldi, D.L. Medina, and A. Ballabio. 2013. Signals from the lysosome: A control centre for cellular clearance and energy metabolism. *Nat. Rev. Mol. Cell Biol.* 14:283–296. https://doi.org/10.1038/nrm3565

Shin, N., H. Soh, S. Chang, D.H. Kim, and C.-S. Park. 2005. Sodium permeability of a cloned small-conductance calcium-activated potassium channel. *Biophys. J.* 89:3111–3119. https://doi.org/10.1529/biophysj.105.069542

Soyombo, A.A., S. Tjon-Kon-Sang, Y. Rbaibi, E. Bashllari, J. Bisceglia, S. Muallem, and K. Kiselyov. 2006. TRP-ML1 regulates lysosomal pH and acidic lysosomal lipid hydrolytic activity. *J. Biol. Chem.* 281:7294–7301. https://doi.org/10.1074/jbc.M508211200

Starkus, J.G., L. Kuschel, M.D. Rayner, and S.H. Heinemann. 1997. Ion conduction through C-type inactivated shaker channels. *J. Gen. Physiol.* 110:539–550. https://doi.org/10.1085/jgp.110.5.539

Steinberg, B.E., K.K. Huynh, A. Brodovitch, S. Jabs, T. Stauber, T.J. Jentsch, and S. Grinstein. 2010. A cation counterflux supports lysosomal acidification. *J. Cell Biol.* 189:1171–1186. https://doi.org/10.1083/jcb.200911083

Tu, Y.H., A.J. Cooper, B. Teng, R.B. Chang, D.J. Artiga, H.N. Turner, E.M. Mulhall, W. Ye, A.D. Smith, and E.R. Liman. 2018. An evolutionarily conserved gene family encodes proton-selective ion channels. *Science*. 359:1047–1050. https://doi.org/10.1126/science.aao3264

Van Dyke, R.W. 1993. Acidification of rat liver lysosomes: Quantitation and comparison with endosomes. *Am. J. Physiol.* 265:C901–C917. https://doi.org/10.1152/ajpcell.1993.265.4.C901

Wang, Q., Z. Wang, Y. Wang, Z. Qi, D. Bai, C. Wang, Y. Chen, W. Xu, X. Zhu, J. Jeon, et al. 2023. A gain-of-function TPC2 variant R210C increases affinity to PI(3,5)P(2) and causes lysosome acidification and hypopigmentation. *Nat. Commun.* 14:226. https://doi.org/10.1038/s41467-023-35786-9

Wang, S., S.-J. Lee, G. Maksaev, X. Fang, C. Zuo, and C.G. Nichols. 2019. Potassium channel selectivity filter dynamics revealed by single-molecule FRET. *Nat. Chem. Biol.* 15:377–383. https://doi.org/10.1038/s41589-019-0240-7

Weinert, S., S. Jabs, C. Supanchart, M. Schweizer, N. Gimber, M. Richter, J. Rademann, T. Stauber, U. Kornak, and T.J. Jentsch. 2010. Lysosomal pathology and osteopetrosis upon loss of H^+-driven lysosomal Cl- accumulation. *Science*. 328:1401–1403. https://doi.org/10.1126/science.1188072

Wie, J., Z. Liu, H. Song, T.F. Tropea, L. Yang, H. Wang, Y. Liang, C. Cang, K. Aranda, J. Lohmann, et al. 2021. A growth-factor-activated lysosomal K(+) channel regulates Parkinson's pathology. *Nature*. 591:431–437. https://doi.org/10.1038/s41586-021-03185-z

Xu, H., and D. Ren. 2015. Lysosomal physiology. *Annu. Rev. Physiol.* 77:57–80. https://doi.org/10.1146/annurev-physiol-021014-071649

Ye, S., Y. Li, and Y. Jiang. 2010. Novel insights into K^+ selectivity from high-resolution structures of an open K^+ channel pore. *Nat. Struct. Mol. Biol.* 17:1019–1023. https://doi.org/10.1038/nsmb.1865

Zhang, J., W. Zeng, Y. Han, W.-R. Lee, J. Liou, and Y. Jiang. 2023. Lysosomal LAMP proteins regulate lysosomal pH by direct inhibition of the TMEM175 channel. *Mol. Cell*. 83:2524–2539.e7. https://doi.org/10.1016/j.molcel.2023.06.004

Zheng, W., C. Shen, L. Wang, S. Rawson, W.J. Xie, C. Nist-Lund, J. Wu, Z. Shen, S. Xia, J.R. Holt, et al. 2022. pH regulates potassium conductance and drives a constitutive proton current in human TMEM175. *Sci. Adv.* 8:eabm1568. https://doi.org/10.1126/sciadv.abm1568

Zhou, Y., J.H. Morais-Cabral, A. Kaufman, and R. MacKinnon. 2001. Chemistry of ion coordination and hydration revealed by a K^+ channel-fab complex at 2.0 A resolution. *Nature*. 414:43–48. https://doi.org/10.1038/35102009

Supplemental material

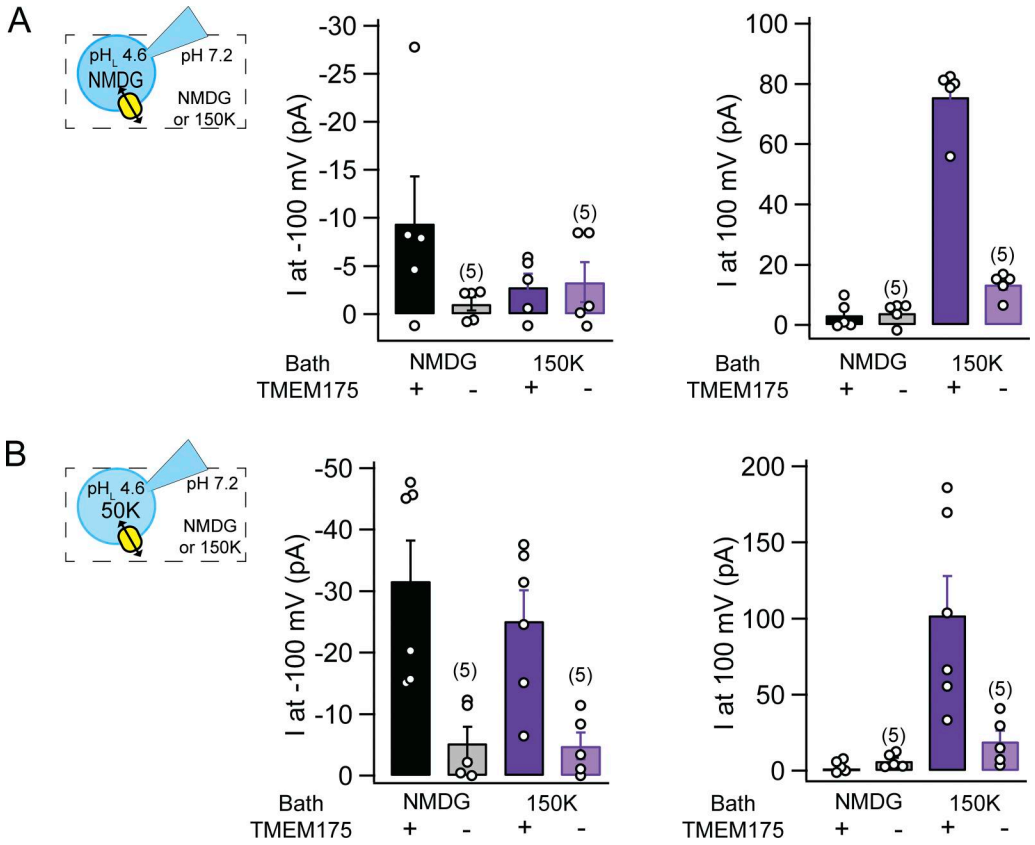

Figure S1. **Lysosomal currents of non-transfected lysosomes/cells with luminal pH 4.6.** Whole lysosomal patch recordings were recorded from lysosomes of nonfluorescent cells on the same coverslips as TMEM175-positive cells to ensure conditions are as similar as possible. **(A and B)** Current amplitudes at −100 and +100 mV obtained with a ramp protocol from −120 to +120 mV in 1 s, Ψ_h = 0 mV with bath solutions containing 0 mM (NMDG-containing) or 150 mM K^+ at pH 7.2 and pipette solutions containing 0 mM (A) or 50 mM K^+ (B). **(A)** The current amplitudes from TMEM175-positive lysosomes are replotted from Fig. 2 B for comparison. Each circle is the response from a lysosome. **(B)** The current amplitudes from TMEM175-positive lysosomes are the same as Fig. 2 D. Each circle is the response from a lysosome. The nonfluorescent lysosomes for both A and B (n = 5). Error bars are SEM.

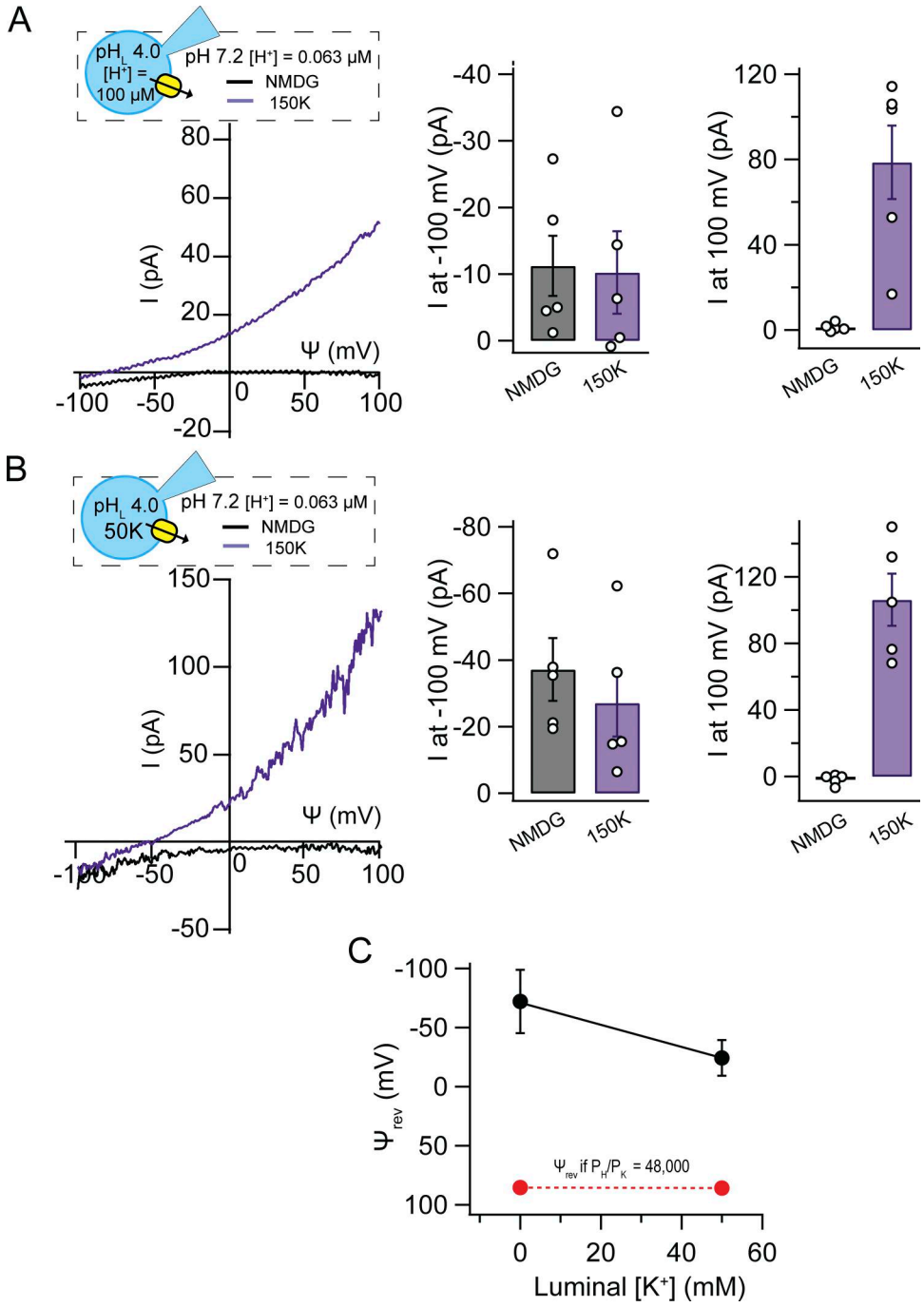

Figure S2. **Lysosomal TMEM175 currents with luminal pH 4.0.** Whole lysosomal patch recordings were from TMEM175-transfected HEK293T cells. *I*-Ψ relationships were obtained with a ramp protocol from −120 to +120 mV in 1 s, Ψ_h = 0 mV. Pipette and bath solutions had pH 4.0 and pH 7.2, respectively. **(A and B)** Currents are recorded with bath solutions containing 0 mM (NMDG-containing) or 150 mM K^+ and pipette solutions containing 0 mM (A) or 50 mM (B) K^+. For each pipette condition, representative traces recorded with NMDG-containing and 150 mM K^+-containing bath from the same lysosome are shown on the left. Summaries of the inward (at −100 mV) and outward (at +100 mV) currents are on the right. Each circle is a response to the respective bath from a lysosomal patch, *n* = 5. **(C)** Average reversal potentials obtained with 150 mM K^+-containing bath and pipette solutions containing 0 or 50 mM K^+, *n* = 4 and 5, respectively. The corresponding calculated P_H/P_K for pH 4.0/NMDG and 150 mM K^+ bath is ∼85 and P_H/P_K for pH 4.0/50K and 150 mM K^+ bath is ∼63. Error bars are SEM.

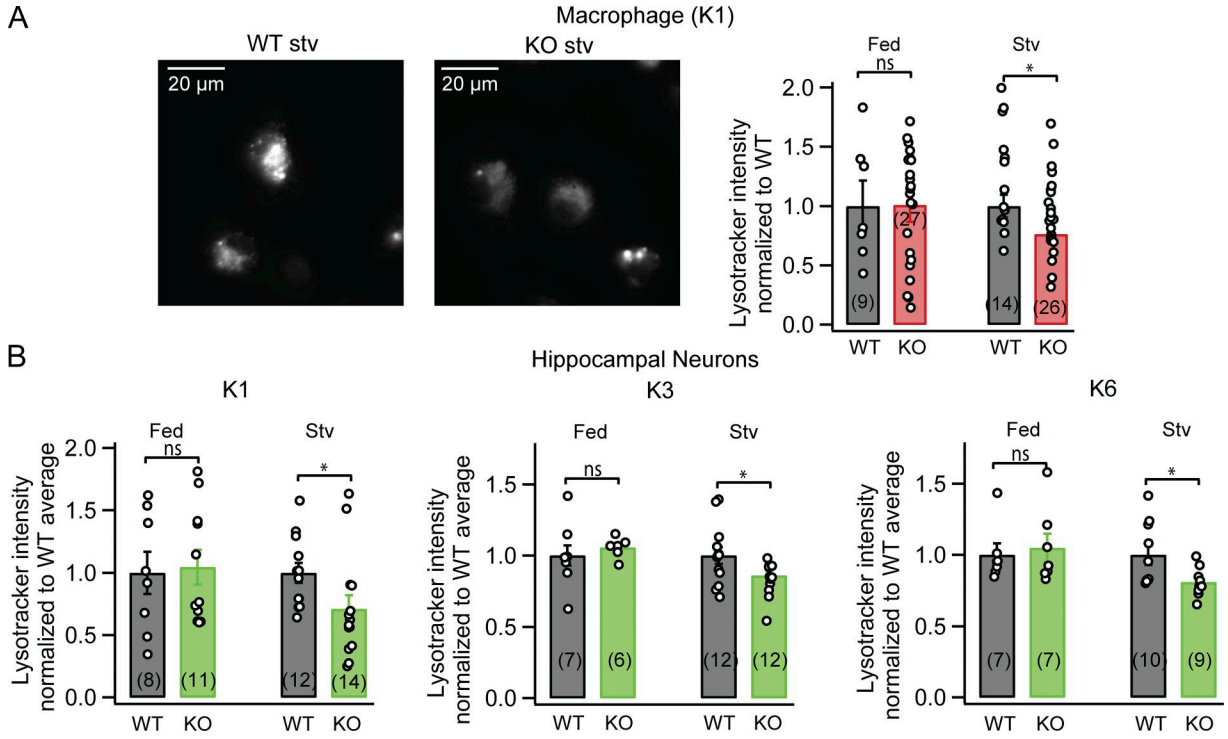

Figure S3. **Alkalinization of TMEM175 KO cells with LysoTracker.** Measured relative fluorescence from cells loaded with LysoTracker, a non-ratiometric, pH-sensitive dye which increases in fluorescence with increased [H^+] or decreased pH. Data were collected in WT and TMEM175 KO pairs for both the fed and starved states. The analyzed LysoTracker intensities were normalized to the value averaged from WT in the same pair. **(A)** LysoTracker data from macrophages. Left: Representative fluorescence signal of WT cells and TMEM175 KO cells in a single field of view with a 20 µm scale bar. Right: Summary of relative LysoTracker fluorescence analyzed by cell in fed and starved WT and TMEM175 KO cells. Numbers in parenthesis are the number of cells analyzed per condition and the circles represent the normalized intensity of one cell. **(B)** Summary of relative LysoTracker intensity analyzed by individual lysosomes and averaged per cell in fed and starved WT and TMEM175 KO hippocampal neurons. Sequence deletions in three independent TMEM175 KO mouse lines (K1, K3, and K6) were used and respectively labeled. Each circle is one cell and over 300 lysosomes were counted in each condition and the numbers in parenthesis are the number of cells. The only significant difference observed is the decrease in fluorescence in TMEM175 KO cells after starvation in both hippocampal neurons and macrophages, consistent with lysosomal alkalinization in the KO. P values are from unpaired two-tailed *t* test, where * is $P < 0.05$ and error bars are SEM.

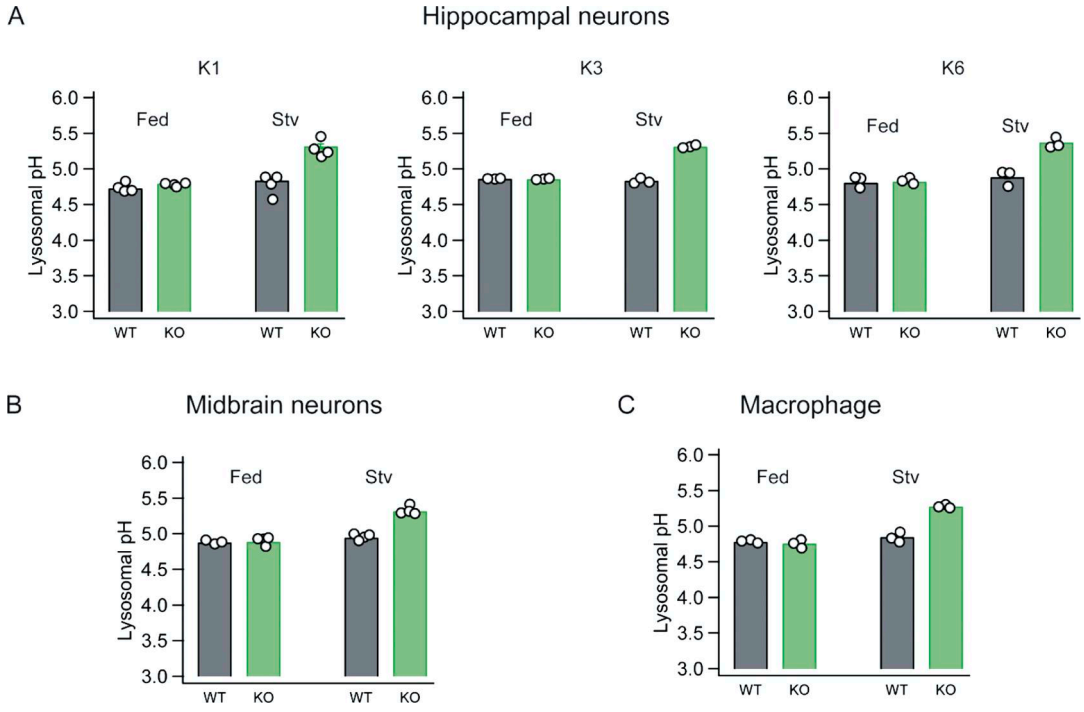

Figure S4. **Lysosomal pH of WT and TMEM175 KO cells by mouse pair. (A–C)** Lysosomal pH measurement of cultured mouse hippocampal neurons (A), midbrain neurons (B), and extracted peritoneal macrophages (C) from WT and TMEM175 KO mice. Each cell culture had at least three pairs of WT and TMEM175 KO mice from at least two litters. Each circle represents the lysosomal pH average of all the cells analyzed from one mouse in both the nutrient-replete and depleted conditions. Error bars are SEM.

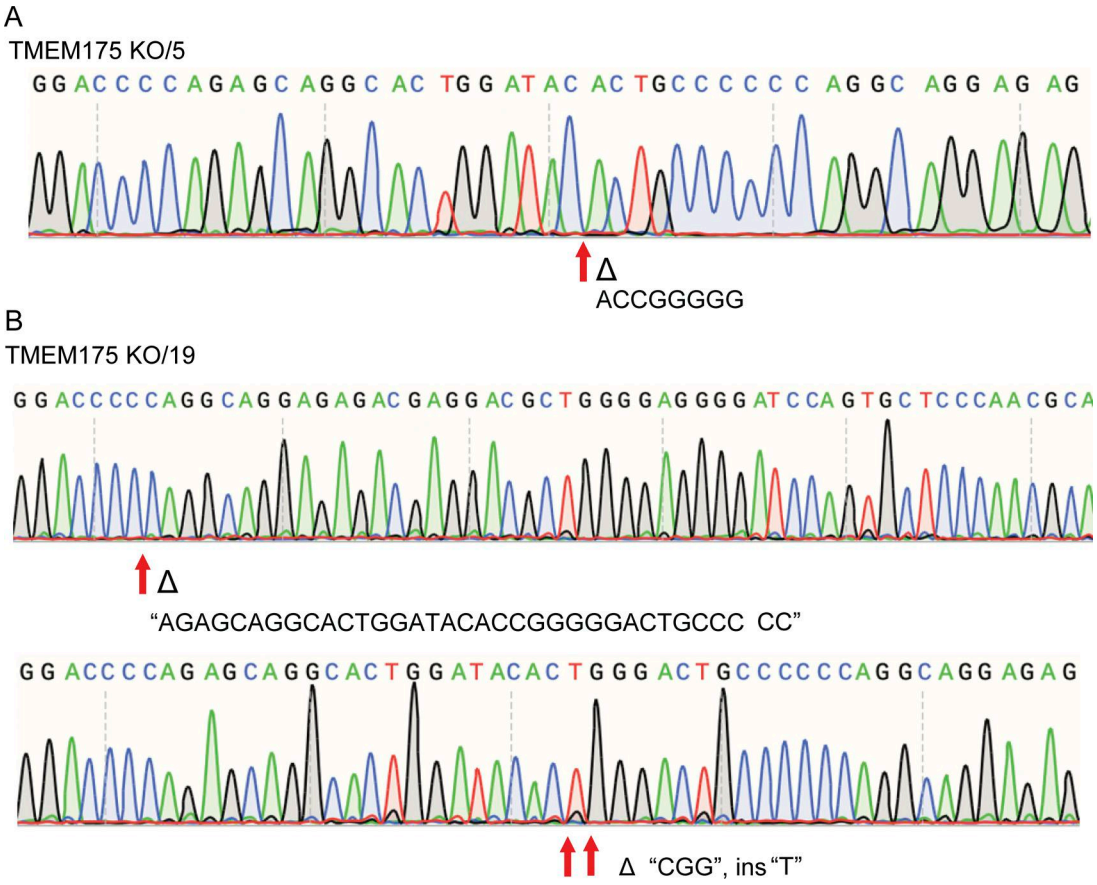

Figure S5. **HEK293T cell TMEM175-KO lines. (A and B)** Sequence deletions in the two TMEM175-KO HEK293T lines with out-of-frame disruptions, TMEM175 KO/5 (A) and TMEM175 KO/19 (B) used in the study. Position of deletion (A) and replacement (B) are indicated by arrows below the Sanger sequencing chromatograms. Sequencing in A was from a cell lysate PCR sample showing a homozygous deletion of 8 bp in the open-reading frame. Clone HEK-KO19 (B) is heterozygous for two alleles with different lengths of deletions, one with 35 bp deleted and the other with 3 bp replaced by an insertion of 1 bp. The sequences are from cell lysate PCR cloned into pBlueScript plasmid vector. Sequence in region of WT is 5′-ACAGGCACACTCAGACCTGCCTTTCCTCCCAGGCTCCTGTAACCG CCAGGCAGCGGCCCCGCCATGTCCCAGCCCCGGACCCCAGAGCAGGCACTGGATACACCGGGGGACTGCCCCCCAGGCAGGAGAGACGAGGACGCTGGGGAGGGGATC CAGTGCTCCCAACGCATGCTCAGCTTCAGTGACGCCCTGCTGTCCATCAT-3′.